Clay Minerals (2026), **61**, 91–119
doi:10.1180/clm.2026.10030

Review Article

Rare earth elements in phyllosilicates

Javier Cuadros[1] and Georgios E. Christidis[2]

[1]Natural History Museum, London, UK and [2]School of Mineral Resources Engineering, Technical University of Crete, Chania, Greece

Abstract

The 14 elements from La to Lu (except the unstable Pm) form a group with similar chemical characteristics provided by their electronic configurations. Widespread, albeit in low abundance (hence their original description as 'rare'), they were soon viewed as an opportunity to trace rock origins and geological processes. In addition to this scientific use, their technological applications have increased over the decades, which have multiplied in the present electronic age. Their exponential growth in demand and limited abundance have transformed them into strategic resources. Characteristic of clay minerals, which take centre stage in so many industrial applications and scientific issues, they have been discovered to be involved in this story as important commercial rare earth element (*REE*) deposits. This review describes how phyllosilicates bind *REE*, how environmental conditions modify *REE* contents in phyllosilicates and how such interactions can be used to trace both original rocks and the nature of modifying geological processes. Phyllosilicates bind *REE* strongly and concentrate them as adsorbed species in inner and outer poly-coordination complexes. This mode of binding controls the capacity for *REE* retention by phyllosilicates in conjunction with the physicochemical conditions of environmental fluids (salinity, pH, temperature, ligands, Eh) and fluid:rock ratios to determine the contribution of clay minerals to bulk *REE* signatures and their modifications in geological processes (soil formation, clay mineral precipitation from fluids, alteration, diagenesis, ore formation, transport).

Keywords: Clay minerals; geological processes; ion-adsorption *REE* deposits; phyllosilicates; rare earth elements; transport processes

(Received 22 October 2025; revised 11 March 2026; Accepted Manuscript published online: 17 April 2026)

Rare earth elements (*REE*) have jumped from the realms of scientific literature and specialized ore geology and industry into the limelight of economy journals and daily conversation. The reasons for this are that *REE* are increasingly used in technology applications in wide circulation (see fig. 1 of Goodenough *et al.*, 2018), while their known sources are limited and there is an increasing supply risk (Goodenough *et al.*, 2018). In a word, they have become critical mineral resources (Chakhmouradian & Wall, 2012). The greater part of these supplies is located in China (~40% of the estimated global resources, followed by Vietnam and Brazil with ~20% each; USGS, 2022), which has prompted governments to find alternative deposits that may supply the market and decrease the risks associated with concentrated sources.

REE concentrate in phosphates (e.g. monazite, xenotime and apatite), fluorocarbonates (e.g. bastnäsite, synchysite and parisite) and oxides (e.g. loparite and fergusonite). Typical *REE* deposits comprise carbonatites, pegmatites, granites, hydrothermal-metasomatic rocks, placers and laterites (Chakhmouradian & Wall, 2012). *REE*-rich clay minerals are found in laterites. Phyllosilicates of magmatic or metamorphic origin retain *REE* but do not significantly concentrate them. The process by which *REE* are concentrated in phyllosilicates of alteration origin (laterites) is by retention of *REE* released from other minerals during weathering, especially *REE*-rich minerals.

In principle, ore mining requires 'high' ore concentrations or inexpensive recovery procedures to ensure financial benefit. The former is rarely the case with *REE*. However, although typically present at concentration levels of only parts per million, *REE* are ubiquitous in the Earth's crust. As discussed in this review, their ubiquity and similar chemical behaviour make them scientifically valuable because they can be used as tracers of precursor rocks and geological processes, as their concentration patterns are partly inherited and partly modified throughout the sequence of geological events, including those involving extraterrestrial materials (Martínez-Ruiz *et al.*, 2006). Because phyllosilicates (of all crystal sizes) are also ubiquitous, generally abundant (McLennan, 2001) and have a significant affinity for *REE* (Liu *et al.*, 2022), they are also a significant *REE* reservoir and play an important role in shaping *REE* concentration patterns across geological processes and rock or sediment evolution (McLennan, 2001; Liu *et al.*, 2021; Andrade *et al.*, 2022). This review describes the partnership between *REE* and phyllosilicates in the light of corroborated research and recent developments, with the intent of stimulating interest in studies that further advance our understanding of geological cycles on Earth and beyond. The expressions 'phyllosilicates' and 'clay minerals' are used throughout this paper with the same meaning, albeit conveying an emphasis on larger particle size and finer particle size, respectively.

Corresponding author: Javier Cuadros; Email: j.cuadros@nhm.ac.uk

Cite this article: Cuadros J and Christidis GE (2026) Rare earth elements in phyllosilicates. *Clay Minerals* **61**, 91–119. https://doi.org/10.1180/clm.2026.10030

© The Author(s), 2026. Published by Cambridge University Press on behalf of The Mineralogical Society of the United Kingdom and Ireland. This is an Open Access article, distributed under the terms of the Creative Commons Attribution licence (http://creativecommons.org/licenses/by/4.0), which permits unrestricted re-use, distribution and reproduction, provided the original article is properly cited.

REE charge and radius

The electronic configurations of *REE* or lanthanides (Ln; i.e. La to Lu except the unstable Pm) in their more external orbitals generate their corresponding valences (Table 1). Obviously, in some cases the loss of three electrons is the most stable ionic form because it produces a noble gas configuration (La, Lu) or a configuration where only the f orbitals of lower energy are filled (Pr to Tb; Suta *et al.*, 2021). From Dy to Yb, the 3+ cations have a configuration in which the higher-energy f orbitals also contain electrons. Yet, there is a constant decrease in the energy of 4f orbitals from La to Lu, which progressively stabilizes electrons in such positions (Peterson & Dyall, 2015). The only two exceptions of geochemical significance to the 3+ valence are Ce^{4+}, which has a noble gas configuration, and Eu^{2+}. Other ionic valences are possible (shown in italics in Table 1, among others) but do not have geochemical relevance. The analysis presented here is a first-order approach to the relative stabilities of the several electron configurations. The full analysis requires a more detailed study of the relative energy levels of orbitals, including the pairing and unpairing of electrons, in specific ligand coordinations, which is not addressed here.

The atomic and ionic radii decrease from La to Lu is due to the increasing attraction of outer-shell electrons by the nucleus. The effect, known as 'Ln contraction', is strongly marked because of the low shielding of the nuclear positive charge afforded by electrons in f orbitals to other electrons in the same and superior shells (Bart, 2023). Because the number of f electrons increases from La to Lu, the poor-shielding effect also increases. Ln contraction has important geochemical consequences because the increasing charge/radius ratio from La to Lu implies that electric attraction of the cations to anionic ligands, and consequent bonding strength, increases in the same series.

Location and mode of retention of *REE* in phyllosilicates

To understand the behaviour of the tandem *REE*–phyllosilicates it is best to address first where and how *REE* bind to phyllosilicates. *REE* cannot be in tetrahedral or octahedral positions in any significant amount because their radii (Ln^{3+}) are greater than those of the usual occupants (e.g. the octahedral radius of Fe^{3+} is 0.65 Å, that of Al^{3+} is 0.54 Å, that of La^{3+} is 1.03 Å and that of Lu^{3+} is 0.86 Å; Laveuf & Cornu, 2009; Cuadros *et al.*, 2023). Work in the 1950s concerned with nuclear waste demonstrated the effective adsorption of Ln on soil and uncharacterized clay minerals (Aagaard, 1974). Later geochemical pioneer work discovered that a large proportion of *REE* in argillaceous sediments (up to 90%) may be adsorbed on clay minerals (Spirin, 1965; Balashov & Girin, 1969; Roaldset, 1973), while the remainder is within mineral crystal sites. This finding raised interest in *REE* adsorption studies on clay minerals. Cormack & Bowen (1967) investigated Ln adsorption on several clay minerals and concluded that such a process could control *REE* concentrations in seawater (as was proven true later). Aagaard (1974) observed that Ln^{3+} ions adsorbed on standard clay minerals with increasing strength as Ln ionic radius decreased (and not with changes to the hydrated Ln radii). Further work demonstrated that Ln^{3+} were exchanged into the interlayer space of montmorillonite, and that complete exchange was achieved in minutes (Bruque *et al.*, 1980). Isotherms of La sorption/desorption in water and X-ray diffraction (XRD) analysis of La-exchanged montmorillonite suggested that La was present as the interlayer complex $La(OH_2)_9^{3+}$ (Mozas *et al.*, 1980).

Table 1. *REE* and their neutral-element external electron configurations, valences and octahedral radii (Å).

	La	Ce	Pr	Nd	Sm	Eu	Gd	Tb	Dy	Ho	Er	Tm	Yb	Lu
Electron configuration	$5d^1\ 6s^2$	$4f^1\ 5d^1\ 6s^2$	$4f^3\ 6s^2$	$4f^4\ 6s^2$	$4f^6\ 6s^2$	$4f^7\ 6s^2$	$4f^7\ 5d^1\ 6s^2$	$4f^9\ 6s^2$	$4f^{10}\ 6s^2$	$4f^{11}\ 6s^2$	$4f^{12}\ 6s^2$	$4f^{13}\ 6s^2$	$4f^{14}\ 6s^2$	$4f^{14}\ 5d^1\ 6s^2$
Valence[a]	3	4, **3**	3	3	**3**, 2	**3**, 2	3	**3**, *4*	3	3	3	**3**, 2	**3**, 2	3
r $(3+)$[b]	1.032	1.01	0.99	0.983	0.958	0.947	0.938	0.923	0.912	0.901	0.890	0.880	0.868	0.861
r $(2+)$[b]						1.17								
r $(4+)$[b]		0.87												

[a]Where there is more than one valence, bold text represents the most stable and frequent valence; regular case represents less stable valences but of geochemical relevance; and italic text represents some other long-recognized valences that are not relevant geochemically.
[b]Radius of the cation with the indicated charge (Shannon, 1976).

https://doi.org/10.1180/clm.2026.10030 Published online by Cambridge University Press

Recently, Borst *et al.* (2020) investigated the chemical environment of Y and Nd, as proxies of light *REE* (*LREE*) and heavy *REE* (*HREE*), respectively, in clay-rich laterite from granite and syenite precursors, using scanning electron microscopy (SEM) and several synchrotron X-ray absorption and fluorescence techniques. They found that *REE* were retained in 8- to 9-coordination water complexes linked to the aluminol surface of kaolinite, from where they were easily removed, as Mozas *et al.* (1980) had suggested for montmorillonite. The hydration complexes found by Borst *et al.* (2020) on kaolinite were the same as in solution, in which nine water molecules are preferred for *LREE* (of greater radius) and eight water molecules are preferred for *HREE* (of smaller radius; Ohta *et al.*, 2008). The same results were reported for *REE* deposits from weathered granite in south Japan containing biotite, smectite and kaolinite, where the exchangeable portion of *REE* approximately corresponded to outer-surface complexes with an extended X-ray adsorption fine structure (EXAFS) spectrum comparable to that in solution (Y was used as a proxy for *REE* in the EXAFS study), while the non-exchangeable portion was mainly in phosphates (Yamaguchi *et al.*, 2018).

The above results suggest that the type of *REE* adsorption is the same for all phyllosilicates, and rather independent of the adsorption site (i.e. interlayer space, layer edges or external planar surface). Other studies seem to corroborate this observation. Slade *et al.* (1998) described La-exchanged vermiculite at ambient conditions as forming an ordered hydration complex where eight water molecules coordinated La as distorted cubes, with two molecules (in opposite corners) buried within the vermiculite ditrigonal cavities. The 001 *d*-spacing was ∼1.5 nm. Olivera-Pastor *et al.* (1988) found the 001 *d*-spacing of Ln-vermiculite to range from 1.51 to 1.47 nm in a series from Ce to Lu, while Iannicelli-Zubiani *et al.* (2015) reported a 001 *d*-spacing for La-montmorillonite just below 1.6 nm. Also for La-montmorillonite, Trillo *et al.* (1992) found the 001 *d*-spacing at 25°C to be 1.57 nm, and X-ray adsorption near-edge structure (XANES) and EXFAS analysis again indicated an interlayer complex of nine water molecules surrounding each La^{3+} ion. Miller *et al.* (1982) observed the 001 *d*-spacing for Eu-, Ho- and Yb-montmorillonite to be 1.52 nm at 20°C and pH ∼6 using 0.1 M Ln solutions. At this temperature, 20% of Eu, 31% of Ho and 37% of Yb were irreversibly retained on the montmorillonite, while these proportions increased with heating of the air-dried specimens, reaching up to 98% at 280°C. Such a drastic increase of *REE* retention with increasing temperature was also observed by Mozas *et al.* (1980). Infrared spectra from Miller *et al.* (1982) showed OH bands at 690–710 and 2680 cm^{-1}, assigned by them to OH bending and stretching in Ln hydroxide (formula not specified), which they interpreted as accounting for the irretrievable Ln. The 2680 cm^{-1} band increased in intensity after heating at 300°C. Studies with clastic rocks indicated that *REE* in illite are also mobile (Uysal & Golding, 2003), suggesting similar complexes of oxygen and hydroxyls from illite layer edges as well as water with the *REE*, or at least with the same binding strength. Alshameri *et al.* (2019) compared the retention of La and Yb in several phyllosilicates, finding the maximum for montmorillonite, then muscovite (∼1/2 of montmorillonite), illite (∼1/4 of montmorillonite) and kaolinite (∼1/8 of montmorillonite). The Ln were desorbed in minutes by cation exchange (with $(NH_4)_2SO_4$), and the recovery was maximal for kaolinite (90%), followed by illite (85%), montmorillonite (80%) and muscovite (60%). This study indicated that at pH 4.0–6.5 (controlled by the clay minerals) the interlayer hosted most of the Ln ions and that the number of surface binding sites was strongly dependent on the density of the surface charge. These results were possibly modified to a varying extent by minor mineral contamination.

Multiple studies have systematically investigated pH effects on *REE* retention by phyllosilicates. The study of Bradbury & Baeyens (2002) on Eu^{3+} exchange for Ca and Na in montmorillonite described greater numbers and types of adsorption sites than the studies mentioned above. Bradbury & Baeyens (2002) modelled the exchange phenomena using multiple types of sorption sites: Eu^{3+} in the interlayer (identical to fully hydrated $Eu(OH_2)_{8-9}{}^{3+}$) and layer-edge sites, the latter being both mono- and bidentate of strong and weak binding character. The edge sites were the following: monodentate = $\equiv S_S{-}OEu^{2+}$, $\equiv S_S{-}OEuOH^{+}$, $\equiv S_S{-}OEu(OH)_3{}^{-}$, $\equiv S_W{-}OEu^{2+}$; and bidentate = $(\equiv S_S{-}O)_2Eu^{+}$, $(\equiv S_S{-}O)_2Eu(OH)_2{}^{-}$, $(\equiv S_W{-}O)_2Eu^{+}$; where ≡S-O denotes smectite edge site and the subscripts 'S' and 'W' denote strong and weak binding sites, respectively. The use of interlayer Eu with only the monodentate or only the bidentate group of sites modelled Eu adsorption similarly well. The proportion of operative sites depended on the concentration of Eu in solution (and pH, as discussed below), so that at pH ∼7 and below $\sim10^{-5}$ M Eu in the equilibrium solution, edge sites lodged more Eu than the interlayer, while interlayer Eu was completely dominant above $\sim10^{-3}$ M. The study of Alshameri *et al.* (2019) mentioned above used concentration ranges of 5.8×10^{-5} to 7.2×10^{-4} M of La and Yb, which is in agreement with smectite having the largest Ln retention among the phyllosilicates tested because it is the only one with interlayer space available for cation exchange.

Qiu *et al.* (2022a) studied Nd, Eu and Lu adsorption on halloysite and illite from initial pH 2–6, which became pH 2.5–5.0 at equilibrium. Adsorption increased from pH 2 to 4 and then became approximately constant up to pH 6. Desorption (using $(NH_4)_2SO_4$) decreased to a varying extent with increasing pH (from 2 to 6) for halloysite and illite. Where complete desorption was achieved, the time needed to reach it was 4–60 min. Olivera-Pastor *et al.* (1988) found the same behaviour with vermiculite at pH 2–5, although Ln adsorption increased at pH 5–7. This increased Ln adsorption surpassed exchange capacity, which was interpreted as being due to water hydrolysis and precipitation of $Ln(OH)_3$. Feng *et al.* (2021) observed that *REE* adsorption on kaolinite at pH 7–13 had two local maxima at pH 10 and 13. Based on X-ray photoelectron spectroscopy (XPS) data, they interpreted retention as $Ln(OH)_n{}^{(3-n)+}$ complexes electrostatically bound to surface sites, where $n = 1$–3 but mainly $n = 2$. Takahashi *et al.* (1998) used laser-induced fluorescence spectroscopy of Eu^{3+} adsorbed on montmorillonite and kaolinite at varying pH values, which showed the following results. On montmorillonite, at pH 1–6 nine water molecules surrounded Eu (equivalent to a fully hydrated state), whereas at pH 6–8 only three water molecules surrounded Eu. In the latter coordination it was considered that OH and/or O from montmorillonite were also linked to Eu, completing the ∼9 coordination (i.e. there were inner-sphere complexes of partially hydrated Eu). At pH 8–12 two phases were present: one with two to three water molecules, the other possibly a hydroxide. On kaolinite, nine water molecules hydrated Eu at pH 2–4. At pH 4–6, there were six to eight water molecules in the coordination sphere, suggesting a simple decreased coordination (for eight water molecules) and additional binding to kaolinite O or OH groups (for six water-coordinating molecules). No information was provided for pH 6–12. Using time-resolved laser fluorescence spectroscopy of Eu^{3+} adsorbed on montmorillonite and kaolinite, Stumpf *et al.* (2002) also reported similar results, with some variations. At pH 3.5–4.0 there was hydration with nine coordinating water molecules for both minerals. At higher pH values there was

https://doi.org/10.1180/clm.2026.10030 Published online by Cambridge University Press

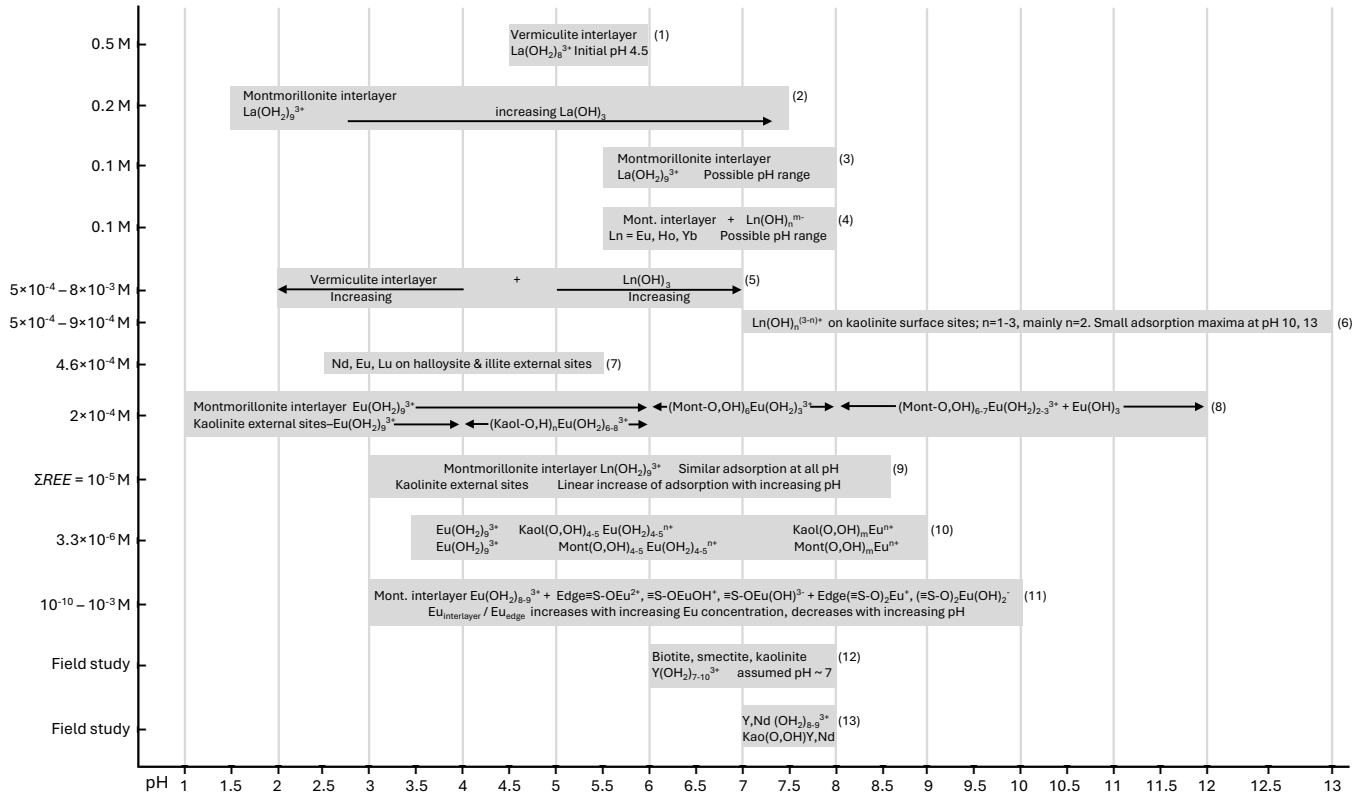


Figure 1. Summary of results from *REE* adsorption studies on clay minerals presented in the article. *REE* concentrations are in the ordinate, while pH values are on the abscissa. The two bottom studies were carried out in the field. The shaded areas indicate the total pH range investigated, and the arrows indicate the specific range over which various Ln species were detected. Where a plus sign appears between species, all of them were found at the same pH range. References: (1) Slade *et al.* (1998), (2) Mozas *et al.* (1980), (3) Trillo *et al.* (1992), (4), Miller *et al.* (1982), (5) Olivera-Pastor *et al.* (1988), (6) Feng *et al.* (2021), (7) Qiu *et al.* (2022a), (8) Takahashi *et al.* (1998), (9) Coppin *et al.* (2002), (10) Stumpf *et al.* (2002), (11) Bradbury & Baeyens (2002), (12) Yamaguchi *et al.* (2018), (13) Borst *et al.* (2020). Kaol = kaolinite; Mont = montmorillonite.

an increasing proportion of inner-sphere ligands in the Eu coordination complex, with 50% inner-sphere complexation at pH 5.5 for kaolinite and pH 6 for smectite, and complete inner-sphere complexation at pH 8–9 for both minerals.

Absorption experiments using various ionic strengths show the extent of ion competition for adsorption sites. Coppin *et al.* (2002) found that at low ionic strength (0.025 M $NaNO_3$ or $NaClO_4$) adsorption of all 14 Ln (added together rather than separately, with ΣREE ~10^{-5} M) was similar for montmorillonite at pH 3.0–8.5, whereas it increased with pH for kaolinite. This suggests that, in montmorillonite, adsorption was predominantly in the interlayer, because it is independent of pH, whereas in kaolinite it necessarily occurred on external sites, which are the only ones available in this mineral. The experiments at high ionic strength (0.5 M $NaNO_3$ or $NaClO_4$) demonstrated competition between Na and Ln because (1) the total Ln adsorptions decreased, especially for smectite at low pH, and (2) *REE* showed fractionation in both minerals, with lower retention of *LREE* (larger radius) because Na competes more efficiently with them for adsorption sites.

High temperature modifies the hydration state of *REE* in the interlayer of smectite and vermiculite. The 001 *d*-spacing has been reported to remain at 1.2–1.5 nm up to ~300°C and to collapse to 0.96 nm above this temperature (Mozas *et al.*, 1980; Miller *et al.*, 1982; Trillo *et al.*, 1992). This behaviour was attributed to the formation of *REE* hydroxides that were retained in the interlayer up to ~300°C (Mozas *et al.*, 1980; Miller *et al.*, 1982). The thermal analysis of Mozas *et al.* (1980) showed that interlayer water placed between the $REE(OH_2)_{8-9}^{3+}$ complexes was released at lower temperatures (differential thermal analysis peak at ~130°C), and that the *REE* with shorter radii caused a second water release at ~250–300°C that would correspond to the water from *REE* hydroxides. Trillo *et al.* (1992) heated La-montmorillonite up to 700°C and suggested that the heating first generated $La(OH)_3$ (up to ~500°C) and then produced a La_2O_3-like polymer, supposedly laminar to account for the 0.95 nm 001 *d*-spacing. Trillo *et al.* (1992) concluded that heating did not cause migration of the *REE* into the hexagonal cavity within the interlayer nor to the vacant octahedral sites. Miller *et al.* (1982) also found no or very little *REE* migration to vacant octahedral sites. Progressive heating of *REE*-montmorillonite caused increasing fixation of the REE, with 80–98% irretrievable *REE* depending on the Ln (increased fixation from *LREE* to *HREE*), temperature and treatment duration (increased fixation at higher temperatures and longer durations; Mozas *et al.*, 1980; Miller *et al.*, 1982).

Whereas earlier studies interpreted *REE* adsorption increases with pH as being due to precipitation of $Ln(OH)_3$ (Fig. 1; Mozas *et al.*, 1980; Miller *et al.*, 1982; Olivera-Pastor, 1988), most recent works assigned such adsorption increases to the increased availability of negatively charged metal-O^- sites in the phyllosilicates, at the layer edges of 2:1 and 1:1 phyllosilicates and at the basal surfaces of 1:1 phyllosilicates (Fig. 1). Miller *et al.* (1982) provided infrared (IR) evidence for the existence of $Ln(OH)_3$ species from O–H vibration bands. Figure 1 shows that the studies indicated the existence of *REE* hydroxides only for pH ranges reaching high

https://doi.org/10.1180/clm.2026.10030 Published online by Cambridge University Press

values, such as 7–13 (Feng *et al.*, 2021) and 8–12 (Takahashi *et al.*, 1998), or for the higher range of *REE* concentrations in solution (original or at equilibrium: 5×10^{-4}–0.2 M; Fig. 1). The formation of inner-sphere complexes *vs* hydroxides is expected to depend on these two variables and on the availability of inner-sphere sites (i.e. the concentration of clay minerals in the suspension or solid–liquid interface). This latter variable is not considered in this review for simplicity.

The studies above enable the establishment of the following conclusions regarding the site and mode of adsorption of *REE* by phyllosilicates. (1) All *REE* are adsorbed similarly by all phyllosilicates and can be desorbed by ion exchange to a high extent in a matter of minutes. (2) The capacity of adsorbing *REE* is controlled by the available adsorption sites, which themselves are controlled by the surface area and density of the surface negative charge. Smectite and vermiculite have the highest surface areas because the interlayer space is available to *REE*. (3) Adsorption occurs as outer-sphere *REE* species (fully hydrated $Ln(OH_2)_{8-9}^{3+}$) and as inner-sphere species in which *REE* are coordinated partly by O and/or OH from the surface of phyllosilicates and partly by water molecules. (4) The most important single variable controlling the mode of adsorption is pH, where outer-sphere complexes are prevalent from low to neutral pH and inner-sphere complexes are increasingly prevalent towards higher pH values. (5) Interlayer adsorption of *REE* in smectite and vermiculite always occurs as outer-sphere complexes and independently from pH; for all phyllosilicates, adsorption increases with increasing pH because more external O atoms acquire a negative charge and so can bind *REE* as inner-sphere complexes. (6) All other variables being equal, the increase in *REE* concentration in solution promotes higher adsorption in the interlayers of smectite and vermiculite relative to the layer edges. (7) Increasing temperature and loss of hydration water increase the proportion of non-retrievable *REE* by means of ion exchange from montmorillonite (supposedly also from all smectite and vermiculite minerals).

Influence of phyllosilicates on the concentration and distribution of *REE* in rock, sediment and soil

After the descriptions in the above section (see summary in the last paragraph and Fig. 1), it is easier to address the question of how phyllosilicates contribute to the concentrations and patterns of *REE* in rocks. This question, however, has two elements. First, what is the intrinsic behaviour of phyllosilicates in retaining/releasing *REE*? Second, how do different geochemical processes (e.g. weathering, hydrothermal alteration, acidic dissolution, deposition in sea basins, etc.) modify such intrinsic behaviour? The first of these elements is addressed in this section.

To be efficient at modifying rock geochemistry, any geochemical process requires the action of a fluid, typically water. Upon interaction with water, silicate rock will partially dissolve, generating a range of dissolved species and producing new mineral phases, including phyllosilicates. The overall effect on *REE* distribution will result from (1) the pervasiveness of the water–rock interaction (e.g. extent of rock dissolution or alteration) and (2) the competition between retention sites in the several mineral phases, original and neoformed, and in the solution. The total concentration of *REE* may decrease during a geochemical process if *REE* migrate with fluids, or it may increase if there is large rock dissolution and the remaining altered rock is efficient at retaining *REE* from the dissolved rock.

Less commonly, *REE* may increase without rock dissolution because solids scavenge *REE* from fluids. Such a case is rarer because *REE* concentration in fluids is much lower than in rocks (by a factor of 10^{-2}–10^{-7}), with only high-temperature, acidic fluids reaching *REE* concentrations above the level of parts per billion (McLennan, 1989). Consequently, these *REE*-enriching processes require very long times and/or fluids with extremely high *REE* concentrations. Because *REE* redistribution among solid phases and dissolved species (e.g. sulfates, carbonates, OH complexes, water-solvated) depends on the relative number and strength of each of these binding sites, modifications of *REE* concentrations are always to some extent relative to the specific process and conditions in operation.

On a first approximation, phyllosilicates reproduce the *REE* patterns of the original rocks, as shown by Cullers *et al.* (1975). These authors investigated 17 clay minerals originating from various processes and locations, including kaolinite, montmorillonite, chlorite, illite, interstratified illite-smectite, glauconite and vermiculite, as well as the clay fractions from two shales (Lower Permian Havensville and Eskridge shales of Kansas and Oklahoma). Their results showed similar *REE* patterns, although the total *REE* concentrations were fairly variable (less so when normalized to chondrite or North American shale composite (NASC)). The results from Cullers *et al.* (1975) suggested that mineralogy did not modify the *REE* patterns, and that all differences in *REE* concentrations between clay minerals could be ascribed to the inheritance from precursor rocks or to different geochemical processes at their origin, deposition or diagenesis. This conclusion is coherent with the similar mode of retention of *REE* by all clay minerals (i.e. adsorption through multiple O, OH and H_2O sites in the interlayer space and/or crystal surface).

Bayon *et al.* (2015) investigated sediments from 53 rivers worldwide draining watersheds of various geological contexts and watershed areas ranging from 6.3×10^6 to <100 km^2. Sediments were collected from rivers, estuaries or deltas. The aim was to obtain a global view of *REE* of the silt and clay fractions of river sediments. For rivers draining sedimentary, igneous and metamorphic terrains, silts had homogeneous *REE* concentrations, very close to the Post-Archaean Australian Shale (PAAS), proposed by Taylor & McLennan (1985) as an average for the *REE* composition of the continental upper crust. The corresponding clay fractions, however, showed a slight enrichment of *LREE* (maximum *REE*/PAAS ratio of 2) and shallow positive Eu anomalies. The volcanic terrains displayed significantly more variable *REE* patterns and concentrations, except those corresponding to very large basins. Bayon *et al.* (2015) interpreted the slightly different *REE* concentrations in silt and clay fractions as being due to preferential alteration of feldspars (and perhaps accessory phases) into clay-sized material (feldspars typically display a positive Eu anomaly and a slope decreasing from *LREE* to *HREE*; McLennan, 1989). This study also demonstrated that clay minerals retain the *REE* patterns of the original rocks and, to a large extent, even their concentrations. The fine fractions studied by Bayon *et al.* (2015) contained different clay minerals in various proportions.

In another global investigation, McLennan (2001) calculated the average *REE* compositions of the coarse- and fine-grained fractions of clastic sediments of various origins. The coarse sediments displayed *REE* compositions coincident with the upper continental crust (UCC), whereas the fine sediments, although closely replicating the same patterns, had higher overall concentrations (5–10 times higher). The greater affinity of the fine fractions for *REE* is due to the greater clay mineral content. The large, negatively

https://doi.org/10.1180/clm.2026.10030 Published online by Cambridge University Press

charged surface area of clay minerals retains large amounts of *REE* with significant strength. The presence of minerals containing large proportions of *REE* (e.g. phosphates) would modify the distribution of *REE* depending on their particle size. The investigation of such a possible presence is always part of *REE* studies. Here, such a possibility will be mentioned only in the studies in which they were found.

Such an affinity between phyllosilicates and *REE* has important global consequences. Abbott *et al.* (2019) investigated *REE* concentrations in marine sediment porewaters and the mineralogy and particle size of the sediments, and they concluded that the most likely control on seawater *REE* composition is the balance between clay mineral dissolution and neoformation in sea sediments (as proposed by Cormack & Bowen, 1967). The requirements for such control are (1) the presence of large amounts of clay minerals in the sediments and (2) that clay minerals retain a large proportion of *REE*, both of which are fulfilled. The results by Abbott *et al.* (2019) are reproduced here in a plot combining several datasets (Fig. 2a). The overall river-suspended material from Viers *et al.* (2008) is compared with the corresponding clay and silt fractions of Bayon *et al.* (2015). However, because the overall river-suspended material was thought to be substantially modified by the presence of *REE*-rich phosphate (Viers *et al.*, 2008), we subtracted the *REE* signature of monazite (Mariano, 1989; McLennan, 1989), after dilution (900 times), from the overall river-suspended material. The result, as expected, is a bulk suspended sediment with lower *REE* than silt or clay (Fig. 2a), because *REE* concentrate in the fine fractions of sediments (McLennan, 1989).

In consequence, dissolution of detrital phyllosilicates in sea basins, typically in the finer sediment fractions, should release large amounts of *REE*, while the formation of authigenic phyllosilicates in such basins should retrieve proportional but lower amounts. The net difference would correspond to *REE* dissolved in seawater. Because phyllosilicates have a *REE* affinity that is slightly different from that of other silicates, the dissolution–neoformation cycles will result in an *REE* signature of porewater that is provided by the phyllosilicates. The specific *REE* signature that the clay minerals confer to seawater has been assessed. Values from Abbott *et al.* (2019; Tasman Sea values in Fig. 2a) and Bayon *et al.* (2023; Fig. 2b) show that seawater and marine sediment porewaters most frequently contain *HREE* > *MREE* > *LREE* (where *M* stands for 'medium'), which suggests that the *REE* signature of seawater is indeed produced by clay mineral dissolution (i.e. the dissolution of the finest components of the sediment). Moreover, the pattern of *REE* loss from detrital kaolinite undergoing glauconitization is very similar to the average seawater *REE* distribution (Fig. 2b; Bayon *et al.*, 2023), suggesting that cycles of clay mineral dissolution–neoformation in sea sediments control seawater *REE* composition.

Glauconite is also relevant for discussion here from a different perspective. Because glauconite is most typically an authigenic mineral from marine sediments, it might be possible that the *REE* contribution from detrital minerals to glauconite is attenuated. This, however, is not the case. Glauconite's *REE* signature is controlled by detrital minerals (Fleet *et al.*, 1980; Huggett *et al.*, 2017; Bayon *et al.*, 2023) or cogenetic phosphates (Tóth *et al.*, 2010), even if in complex ways. For example, the signature from the silicate detrital component may combine with that of *REE*-rich phosphate traces (Huggett *et al.*, 2017), and the latter may become increasingly dominant with glauconite maturation due to the concomitant silicate dissolution, while phosphates are entirely retained (Tóth *et al.*, 2010; Bayon *et al.*, 2023). It is also a possibility that the abundant organic matter (OM) of the settings where glauconite grows influences the *REE* signature. OM from sediments (Freslon *et al.*, 2014; Pourret & Tuduri, 2017), including the oceans, displays a PAAS-normalized *REE* pattern with a maximum at Eu and two gently decreasing slopes towards *LREE* and *HREE*, only broken by a frequent shallow Ce positive anomaly, sometimes inexistent or negative (Fig. 3a). These patterns are similar to those displayed by glauconite (Fig. 3b), suggesting that OM may also influence its *REE* signature. Accordingly, glauconite's *REE* contents are controlled by the substrate from where it forms, including both the mineral (sediment) and organic (detritus) components.

In summary, the *REE* concentration in the world-average silt plus clay fractions of river-suspended sediments of Bayon *et al.* (2015) can be assumed to correspond approximately to the average *REE* signature of phyllosilicates: reproduction of the original silicate rock (the average continental crust) with a slightly increased content of *HREE* due to the greater affinity for these *REE* of smaller radius. However, if phyllosilicates are separated into the silt and clay fractions, the relative *LREE*/*HREE* concentration in the clay fraction may be slightly higher in *LREE* due possibly to the finest fraction preferentially containing the clay mineral products of plagioclase alteration, because in plagioclase *LREE* > *HREE* (McLennan, 1989).

Geological modification of *REE* patterns in phyllosilicates

The inertia of phyllosilicates to inherit their *REE* patterns from their precursor silicate rocks is broken when the alteration processes to which they are subjected are 'intense'. In those cases, phyllosilicate transformation produces *REE* pattern modifications, as illustrated by Uysal & Golding (2003) in smectite illitization in the northern and southern areas of the Australian Bowen Basin. They observed that illitization increased *HREE*/*LREE* ratios. However, in the northern Bowen Basin such an increase was due to a decrease in *LREE* with illitization, while in the southern Bowen Basin this was due to an increase in *HREE*. In the northern Bowen Basin, illitization did not correlate with temperature but rather with an increase in the water/rock ratio and/or K concentration in the interstitial fluids, which are also variables controlling smectite illitization (Howard & Roy, 1985; Whitney, 1990; Cuadros, 2006). In the southern Bowen Basin, the water/rock ratio was lower and temperature controlled the reaction, as shown by its good correlation with illite content (Uysal & Golding, 2003). In the northern Bowen Basin, a high water/rock regime meant that many fluid-borne binding sites were competing for *REE* with the transforming smectite, and, at the same time, K concentration was driving the reaction forward. Because *HREE* bind to phyllosilicates more strongly than *LREE* due to their higher charge/radius ratio (Chakhmouradian & Wall, 2012), a decrease in *LREE* was the logical outcome of the interaction with waters in which both the water/rock ratio and K concentration increase together, because both variables promote dislodging of *REE* and are more efficient at doing so with *LREE*.

As for the southern Bowen Basin, where the water/rock ratio was low, Uysal & Golding (2003) suggested that the increase in *HREE* was due to the assumed (but not measured) high pH and high alkalinity of the hydrothermal fluids that would enrich them in *HREE*. In our opinion, there is no need to have recourse to an assumed alkalinity of the fluids. We propose an interpretation with elements relevant to understanding *REE* signatures in phyllosilicates generally. Uysal & Golding (2003) determined *REE* values in the concentrated clay fractions (<0.2 μm of mudrocks and sandstones and <2 μm of bentonites), so their *REE* results

https://doi.org/10.1180/clm.2026.10030 Published online by Cambridge University Press

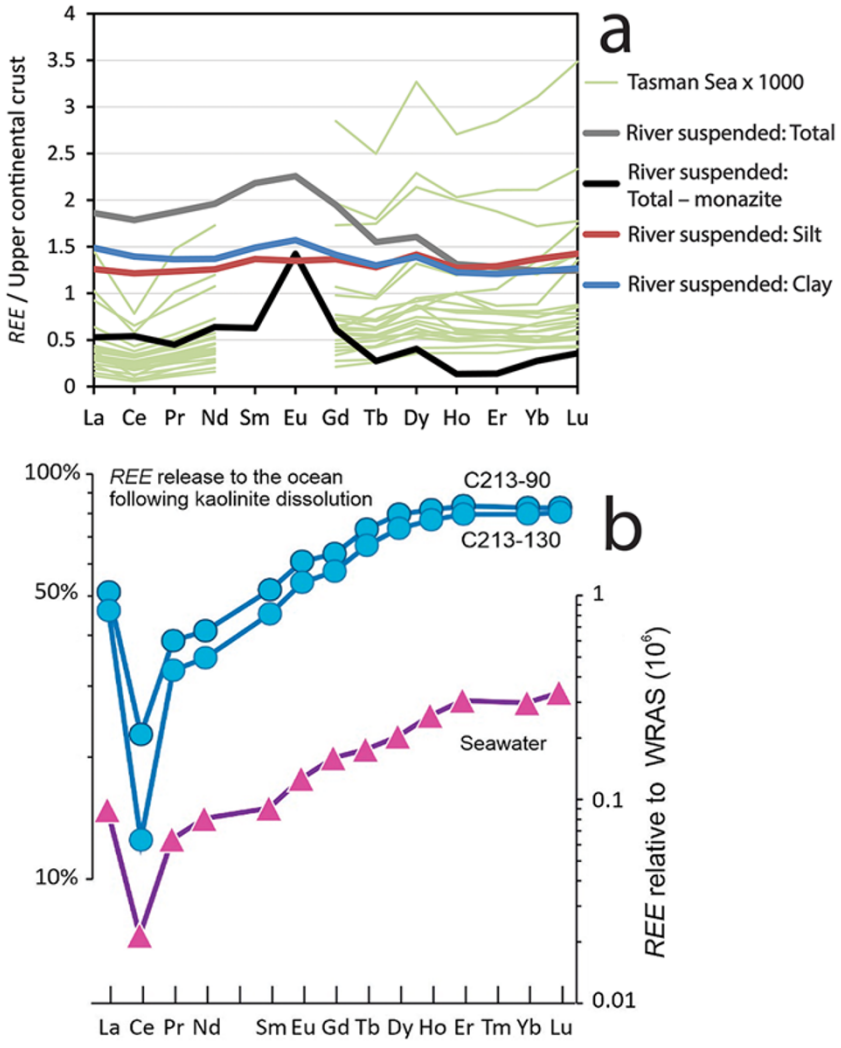


Figure 2. *REE* concentrations in detrital marine sediments and seawater. (a) Grey line: average *REE* in river-suspended sediments from Amazon rivers (Viers *et al.*, 2008), as representative of world average; black line: the same value after subtraction of *REE* in suspected monazite (monazite *REE* composition assessed from Mariano, 1989; McLennan, 1989; 900 times dilution); red and blue lines: world-average *REE* in river-suspended silt (red) and clay fractions (Bayon *et al.*, 2015); green lines: *REE* in porewaters of the Tasman Sea (Abbott *et al.*, 2019). (b) Blue data points and left-hand *y*-axis: shale-normalized percentage of *REE* content in detrital kaolinite released to seawater during the formation of mature glauconite in two samples from the Congo continental shelf; purple data points and right-hand *y*-axis: *REE* in global seawater normalized to world river average silt (WRAS). The patterns' similarity suggests that clay mineral dissolution controls the seawater *REE* pattern (Bayon *et al.*, 2023).

correspond to illite-smectite only. In the southern Bowen Basin, temperatures ranged from 75°C to 200°C, with the higher temperatures corresponding to the more illitic samples (Uysal & Golding, 2003). The higher range of these temperatures must have caused substantial dissolution of other minerals and the corresponding *REE* release. These released *REE* were in confined solutions (low water/rock regime) and in proximity to the illite-smectite surface, which scavenged them from the solution. Because *HREE* are more efficiently bound by phyllosilicates (higher charge/radius ratio), the proportion of scavenged *REE* increased from *LREE* to *HREE*. In the northern Bowen Basin, as indicated above, the regime was of a high water/rock ratio and *REE* were more readily transported away by the fluids, but this only happened to the *LREE* (not *MREE* or *HREE*), as these are the ones most weakly retained by the illite-smectite.

The conclusion is important: in low-porosity environments phyllosilicates retain the *REE* signal from their precursors or concentrate *MREE* and *HREE* to a moderate extent. In high water/rock regimes, the capacity of fluids to uptake and retain *REE* increases, and the outcome therefore also depends on fluid composition, pH, temperature and any other variable affecting the stability of *REE* in water complexes or *REE* hydroxides (for high pH). *REE* stability in waters is governed by more numerous and more complex variables than *REE* stability on phyllosilicates, so general rules cannot be provided where *REE*–fluid interaction becomes a contributing factor to *REE* behaviour (Williams-Jones *et al.*, 2012). Interestingly, however, the study of Uysal & Golding (2003) produced the same result of an increased ratio of *HREE*/*LREE* in two different water/rock regimes, although due to different causes. In both cases, however, alteration of smectite was 'intense', due to either a high water/rock ratio and K concentration or to high temperature.

To simplify matters, it is best to explore the effects of individual variables of altering fluid on *REE* concentrations. As this exploration progresses, several of these variables can then be combined to observe the overall effect.

Water salinity

The ion content of alteration fluids of any type and environment has the most straightforward effect on the *REE* signature of phyllosilicates. Because *REE* are mainly present in phyllosilicates as adsorbed on interlayer or external sites, they are exchangeable. Phyllosilicates in contact with alteration fluids undergo cation-exchange reactions with the fluids (Coppin *et al.*, 2002). The higher the cation concentration in the fluids, the greater the amount of

https://doi.org/10.1180/clm.2026.10030 Published online by Cambridge University Press

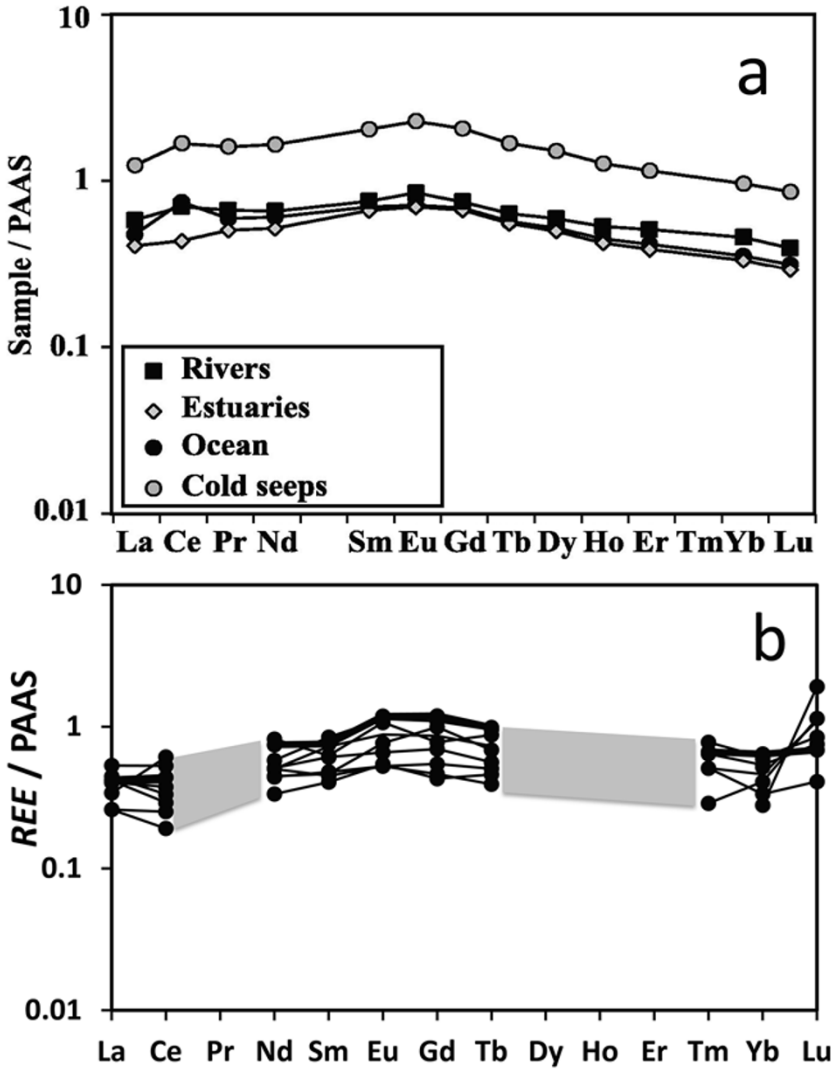


Figure 3. *REE* concentrations normalized to PAAS for (a) OM in sediments of various aqueous environments, including oceans from Freslon *et al.* (2014) and (b) in glauconite collected from the sea floor from Fleet *et al.* (1980). Some *REE* are not analysed, but the trends are shown as lines in (a) and as grey areas in (b).

REE that will be leached from the phyllosilicates in exchange for cations from the solution. In addition, divalent cations are more efficient than monovalent cations at competing with the trivalent *REE* on the phyllosilicates (no trivalent cations of abundant elements (e.g. Al or Fe) exist free in solution at approximately neutral pH because they hydrolyse water and form other species, precipitated or in solution). The cation exchange taking place is rapid and measurable after a short time as a reduction of *REE* in phyllosilicates, to an extent that depends on the variables mentioned in a previous section (Coppin *et al.*, 2002). The relative loss is in the order *LREE* > *MREE* > *HREE* due to the greater bonding strength of *REE* as their radius decreases (from *LREE* to *HREE*; Coppin *et al.*, 2002). However, this effect may be obscured by other phenomena as the contact time between sediment and water increases. The differential dissolution across minerals and particle sizes and the precipitation of new minerals may produce effects on *REE* patterns that contrast with those of simple cation exchange. In practice, simple exchange between sediments or soils and waters, exclusive of any other process, is difficult to detect in natural systems because the time of interaction is typically long enough to allow for other processes to take place. Only experimental studies show simple cation exchange (e.g. Coppin *et al.*, 2002). In summary, water transport of clay mineral sediments or water percolation through them for very reduced periods of time will modify the original *REE* signature of the sediments by reducing their concentration in the order *LREE* > (i.e. more reduced than) *MREE* > *HREE*, perhaps also modifying Ce and Eu concentrations due to their special redox properties.

Fluid pH

Extreme-pH fluids are aggressive to silicates and cause dissolution to an extent that depends on the pH, water/rock ratio and duration of the attack. Many silicate minerals dissolve approximately at the same rate at low and high pH (i.e. their dissolution rates are approximately symmetric on both sides of neutrality; Brady & Walther, 1989; Huertas *et al.*, 1999; Brantley, 2008). Although both low- and high-pH fluids dissolve silicates, their effects on the *REE* of the silicate products are different because the chemistry of the fluids is different (e.g. Li *et al.*, 2022), as discussed below.

Extreme acidity (pH < 3) causes thorough dissolution of silicates, and the resulting fluids reproduce the *REE* signature of the dissolving rock (e.g. Li *et al.*, 2022), as shown in Fig. 4a for pH 1.33–2.50. These specific strongly acidic fluids were at moderate

https://doi.org/10.1180/clm.2026.10030 Published online by Cambridge University Press

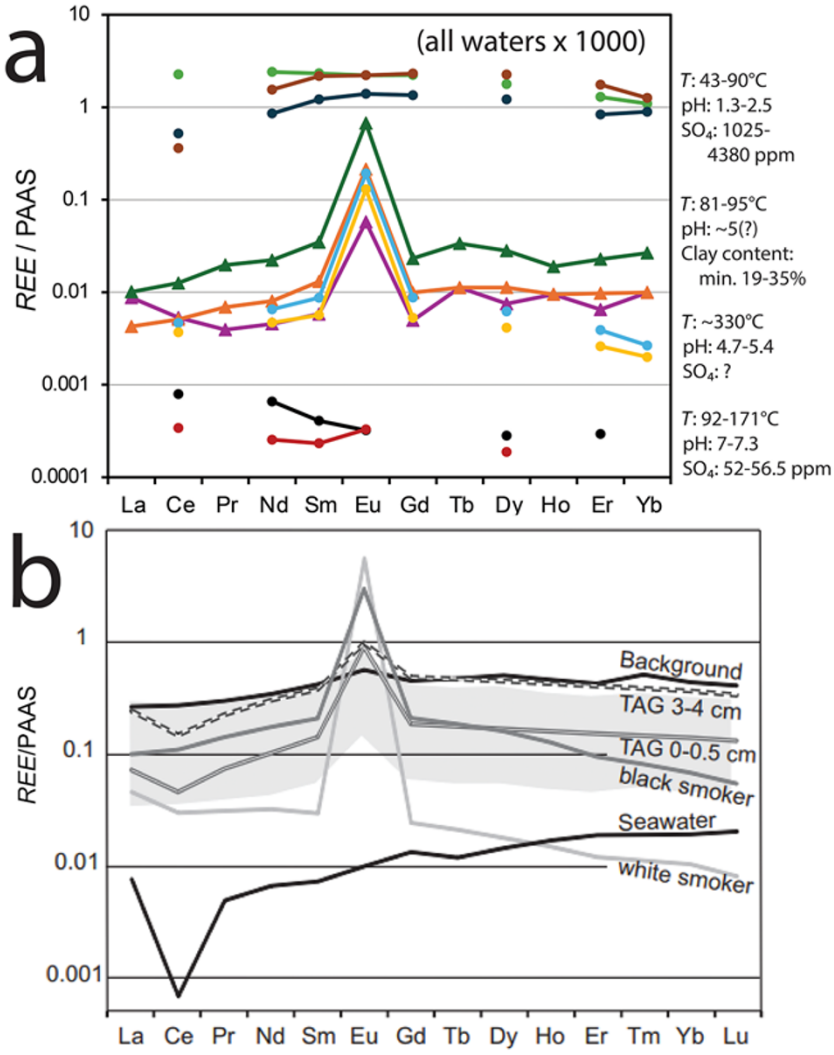


Figure 4. (a) *REE* normalized to PAAS of hydrothermal waters (circles, values ×1000) and hydrothermal sediments (triangles). Three top and two bottom values are from a continental setting in Valles Caldera, New Mexico (Michard, 1989). Two middle water values (yellow and light blue circles) are from the Mid Atlantic Ridge, 23°N field (Mid-Atlantic Ridge at Kane; MARK) (Michard, 1989). Three middle sediment values (triangles) are from the Mid Atlantic Ridge, TAG field (Severmann *et al.*, 2004). (b) *REE* normalized to PAAS of hydrothermal sediments and waters: grey area is a range of composition of Atlantis II sediments (variable composition: Si-, Fe-, Ca- and S-rich), Red Sea, with present brine water temperature of ~67°C and pH 5.4; background sediments are detrital siliceous and biogenic from near the Thetis Deep, Red Sea; TAG are hydrothermal sediments from two depths below the sea floor, Mid Atlantic Ridge; seawater, black smoker (~360°C) and white smoker (~285°C) are all from TAG (from Laurila *et al.*, 2014; their Figure 9c and references therein). The large Eu positive anomaly in fluids and sediments precipitated from the fluids is due to preferential plagioclase dissolution in mildly acidic conditions, whereas in highly acidic and neutral fluids there is total rock dissolution and little non-preferential dissolution, respectively, resulting in no *REE* segregation.

temperatures ranging from 43°C to 90°C (Fig. 4a) and dissolved felsic tuff and tuffaceous sandstone (Nielsen & Hulen, 1984) with approximately flat PAAS-normalized *REE* patterns (e.g. Maslov, 2021). In turn, silicates precipitating from these fluids will approximately preserve the *REE* pattern of the original rock, although at lower concentration (*REE* concentrations of fluids in Fig. 4a are multiplied ×1000). In such conditions, neither dissolution nor neoformation of silicates fractionates *REE*. This is shown in the intense acid alteration of rocks from the Iberian Pyrite Belt, where alteration products with major phyllosilicate contents largely preserve the *REE* patterns of the precursor rocks (Cuadros *et al.*, 2023). Similarly, NASC-normalized *REE* data from a mine with acid drainage also from the Iberian Pyrite Belt (Fig. 5) showed that silicate material where ore was emplaced (ore body waste) displayed the approximately flat *REE* patterns of the background rock, while that of the fully acid-altered rock (gossan), which contained only Fe oxides (no silicates), was of a slightly convex-down shape and of lower concentration. The draining acidic fluids displayed a convex-up shape (as in Fig. 4a at pH 1.3–2.5), complementary to the more attenuated shape of the gossan (Fig. 5). Clay minerals precipitating from such fluids would be expected to have a similar *REE* pattern. In summary, very-low-pH alteration does not modify the *REE* signatures of phyllosilicates except in the case of newly precipitated clay minerals, where *REE* are diluted, and perhaps a slightly convex-up *REE* distribution may develop.

Acid alteration at higher pH does not dissolve the silicate rock homogenously; rather, differential dissolution takes place, whereby some minerals are entirely dissolved, some are altered and others are unaffected. Plagioclase is among the preferentially dissolved minerals, which has a large effect on *REE* distribution, given the high Eu concentration in plagioclase. This high concentration is due to favourable partitioning of Eu in plagioclase during magma crystallization because Eu^{2+} (reducing conditions) substitutes for Ca^{2+} in this mineral. As a consequence, the preferential dissolution of plagioclase generates a large positive Eu anomaly in the fluids, as seen in hydrothermal fluids from the Mid-Atlantic Ridge with pH 4.7–5.4 (Fig. 4a). The same signature is imprinted on neoformed nontronite. However, because the concentration of *REE* in mildly acidic hydrothermal water is very low (*REE* concentrations in fluids are multiplied ×1000 in Fig. 4a), this fractionation does not affect the *REE* concentration in the altered rock, which remains similar to the original (Cuadros *et al.*, 2023; 'MUD' sample in Bobos & Gomes, 2021). Thus, mildly acidic fluids only modify *REE* patterns in newly precipitated clay minerals, generating a strong positive Eu anomaly.

https://doi.org/10.1180/clm.2026.10030 Published online by Cambridge University Press

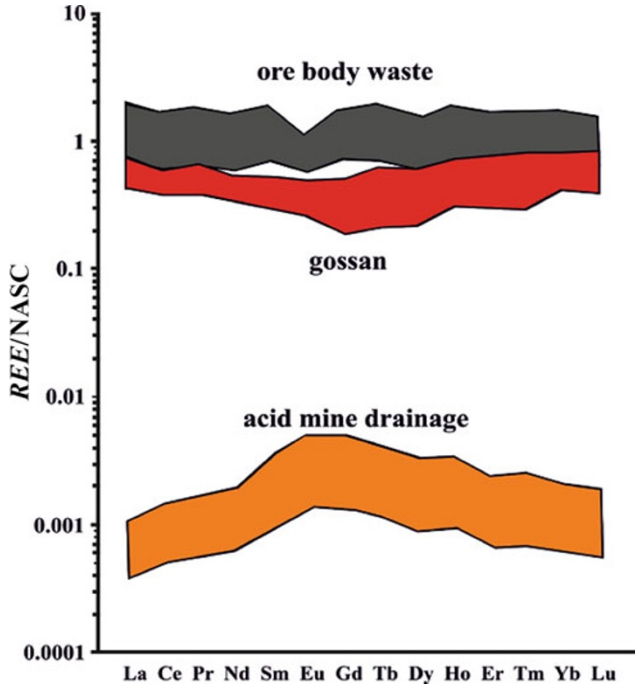


Figure 5. *REE* concentrations normalized to NASC in rocks and fluids of the São Domingos mine, Portugal, within the Iberian Pyrite Belt (Ayora *et al.*, 2015). Ore body waste: acid leached silicate rock; gossan: Fe oxides product of acidic alteration; acid mine drainage: acidic fluids after leaching. Gossan and acid drainage have complementary *REE* patterns (convex down and convex up, respectively).

Neutral to mildly alkaline fluids (pH 7.0–8.6) altering volcanic, clastic-evaporitic and basaltic rock have approximately flat PAAS-normalized *REE* patterns (Fig. 4a), also approximately reproducing those of the precursor rocks. The low *REE* concentrations in the fluids do not significantly modify *REE* contents in the altered rock.

Concentrations of *REE* in terrestrial waters at a wide range of pH values indicate that alkaline waters contain lower concentrations than acidic ones (Fig. 6; the ratio between the two maximum values below and above pH 7 is 12.6; Li *et al.*, 2022). Although, as stated above, a high hydroxyl concentration may dissolve silicates to a similar extent as a high proton concentration, there are no natural mechanisms that can produce OH^- concentrations as high as those of H^+. While sulfuric acid, a strong acid produced by pyrite oxidation, is the most common cause of very acidic environments, there is no such naturally produced strong base. Rather, alkalinity develops from the carbonic–carbonate system, which consists of weak acids and bases, derived from the deprotonation of water. As a consequence, alkaline systems are self-buffered to some extent, and pH $\geq$ 10 is rarely reached (Tosca & Tutolo, 2023).

Most frequently, the shape of the shale-normalized *REE* distributions of alkaline waters is that of progressively increasing values from *LREE* to *HREE*, with or without Ce and Eu anomalies (Fig. 7; Möller & Bau, 1993; Johannesson & Xiaoping, 1997; Sasmaz *et al.*, 2021; Li *et al.*, 2022). More alkaline waters (i.e. more carbonate-rich waters) generally contain higher *REE* concentrations (Johannesson *et al.*, 1995). The positive Ce anomaly that sometimes occurs, in some cases very prominently, is the result of Ce oxidation to Ce^{4+} at high pH (being thermodynamically stable at such conditions) and the formation of very stable $Ce(CO_3)_5^{6-}$ complexes (Möller & Bau, 1993). Pourret *et al.* (2008) modified this interpretation, indicating that OM binds Ce^{4+} more strongly than the penta-carbonate anion and sequesters Ce from the true dissolved phase into the very fine colloidal (organic) phase, resulting in a negative (rather than positive) Ce anomaly in solution and a positive Ce anomaly in the colloidal fraction. The same authors ascribed the variability of Ce behaviour in alkaline pH to the variable concentration of OM in alkaline lakes, where high CO_3^{2-}/OM ratios result in largely dissolved Ce^{4+} (as $Ce(CO_3)_5^{6-}$) and a positive Ce anomaly in the fluid, while low ratios result in largely colloidal Ce^{4+} and a negative Ce anomaly in the solution (Pourret *et al.*, 2008). It follows that the Ce anomaly depends on whether OM is truly dissolved or forms colloids (i.e. it depends on the experimental limit (filter) established for colloid size in its separation from the fluid). The positive Eu anomaly, when it occurs, is caused by preferential dissolution of plagioclase, as in acidic waters (Li *et al.*, 2022). Negative Eu anomalies are derived from the dissolution of the entire rock, without preferential plagioclase dissolution.

Because alkaline waters are saline as a result of the dissolution of carbonates (Tosca & Tutolo, 2023), cations (mainly Ca and Mg) cause partial desorption of *REE* from phyllosilicates. At the same time, alkaline lakes are very productive biologically and contain large microbial populations, both planktonic and within biofilms (Haines *et al.*, 2023; Tutolo & Tosca, 2023). These microbial colonies develop a large surface area of contact with water that results in significant adsorption and sequestration of *REE* by biomass (Takahashi *et al.*, 2007) and biominerals (Kaya *et al.*, 2023). However, the determining factor in controlling *REE* concentration in alkaline waters is carbonate ion concentration, to be discussed below.

Fluid temperature

Increasing temperature increases the solubility of silicates so that the effects on *REE* are similar to those of decreasing pH. However, silicate solubility is more sensitive to lowering pH than to increasing temperature. Lowering of pH from 7 to 5 to 2 is consistently effective at increasing dissolution, whatever the fluid temperature (Fig. 4a). Submarine hydrothermal vents from the East Pacific Rise of neutral to slightly alkaline pH do not mobilize *REE* below 350°C at water/rock ratios $<10^5$ (Michard & Albarède, 1986). High-temperature vents (~285–360°C; Fig. 4a,b) from the Mid-Atlantic Ridge with only slightly acidic pH (4.7–5.4; Fig. 4a) preferentially dissolve plagioclase among the silicates, as shown by the large Eu anomaly in such fluids (Fig. 4a,b), indicating that rock dissolution is not homogeneous across minerals. All of the above cases indicate that lowering pH is more effective at dissolving rock than increasing temperature. Nonetheless, *REE* concentrations are higher and the Eu anomaly less pronounced in the black smoker (~360°C) than in the white smoker (~285°C; Fig. 4b), consistent with a more intense, less selective rock dissolution in the former.

The *REE* patterns of sediments in the Trans-Atlantic Geotraverse (TAG) field of the Mid-Atlantic Ridge (TAG 0–5 cm and 3–4 cm deep; Fig. 4b) and of sediments from the Red Sea (Fig. 4b, grey band) inherit the positive Eu anomaly from the hydrothermal fluids, and those from the TAG field also acquire a negative Ce anomaly from the ocean water (note that fluid *REE* concentrations are multiplied ×1000). The background sediment, of sedimentary rather than hydrothermal origin, displays a shallow positive Eu anomaly and a still-shallower or no Ce negative anomaly. This plot (Fig. 4b) is very illustrative in showing how the *REE* patterns of the hydrothermal sediments of the TAG field have multiple influences: they are shaped by the prominent features of hydrothermal fluids (Eu anomaly) and seawater (Ce

https://doi.org/10.1180/clm.2026.10030 Published online by Cambridge University Press

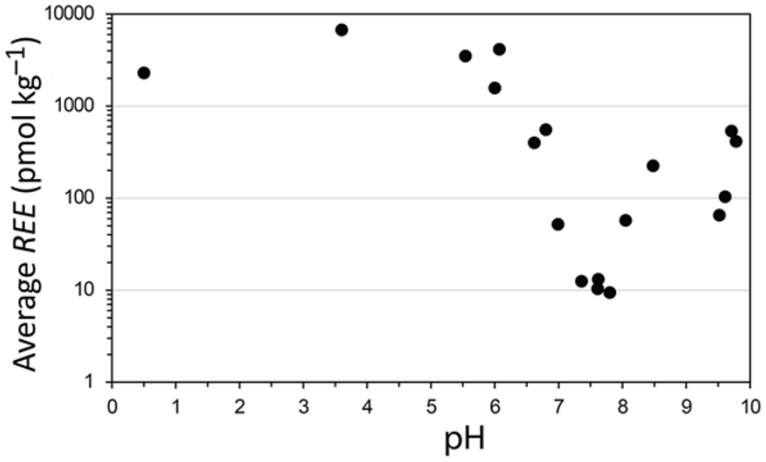


Figure 6. Average concentrations of *REE vs* pH in terrestrial waters. Averages were calculated as $\Sigma REE/n$, where n is the number of *REE* in the calculation. Some *REE* were missing from some of the analyses. The samples include lakes, rivers, groundwaters and springs from Goldstein & Jacobssen (1988), Johannesson *et al.* (1995) and Gammons *et al.* (2005).

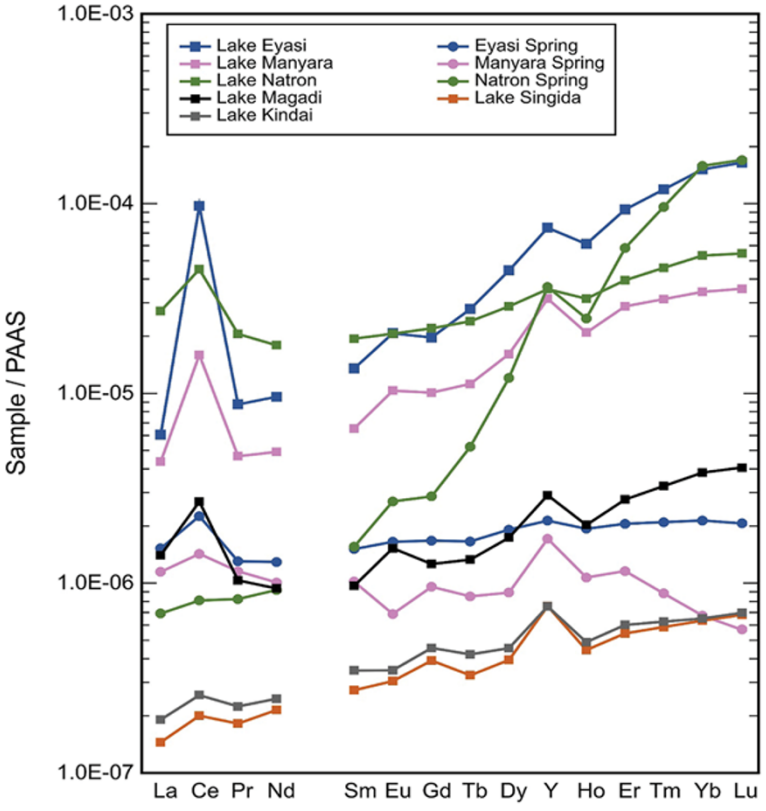


Figure 7. PAAS-normalized *REE* and Y concentration patterns for alkaline lakes (pH 8.9–10.0) and hot springs (pH 9.1–9.7) from Tanzania. Surrounding rocks are *REE*-rich carbonatites. From Kreitsmann *et al.* (2023).

anomaly) while also displaying the slight convex-up shape of the background sediment. There is no negative Ce anomaly in the hydrothermal sediments of the Red Sea (Fig. 4b, grey band) because the background fluids there are not seawater but brines of various composition (Gurvich, 2006).

In summary, high-temperature fluids of neutral pH only mobilize *REE* and fractionate them at rather high temperatures (~300°C and above), with variations depending on the type of silicate rock and the fluid/rock ratio. The fractionation consists of a sharp increase of Eu in the fluid due to selective dissolution of plagioclase. As the temperature increases, all *REE* increase and the Eu anomaly decreases, possibly disappearing at the stage at which dissolution is not selective anymore and all the rock dissolves homogenously. Clay minerals precipitating from fluids at temperature >~300°C have the same *REE* patterns as the fluids: first approximately flat with a large positive Eu anomaly, and then, at much higher temperatures, without an Eu anomaly. Pre-existing phyllosilicates that were altered (not dissolved) by such fluids preserve the *REE* composition of the original rock because the amount of *REE* removed from the rock is negligible (very low *REE* concentration in the fluids). The mechanism of clay mineral neoformation may be (and in many cases is) intermediate between these extremes, and then the *REE* signature will reflect the two sources: rock and fluids.

https://doi.org/10.1180/clm.2026.10030 Published online by Cambridge University Press

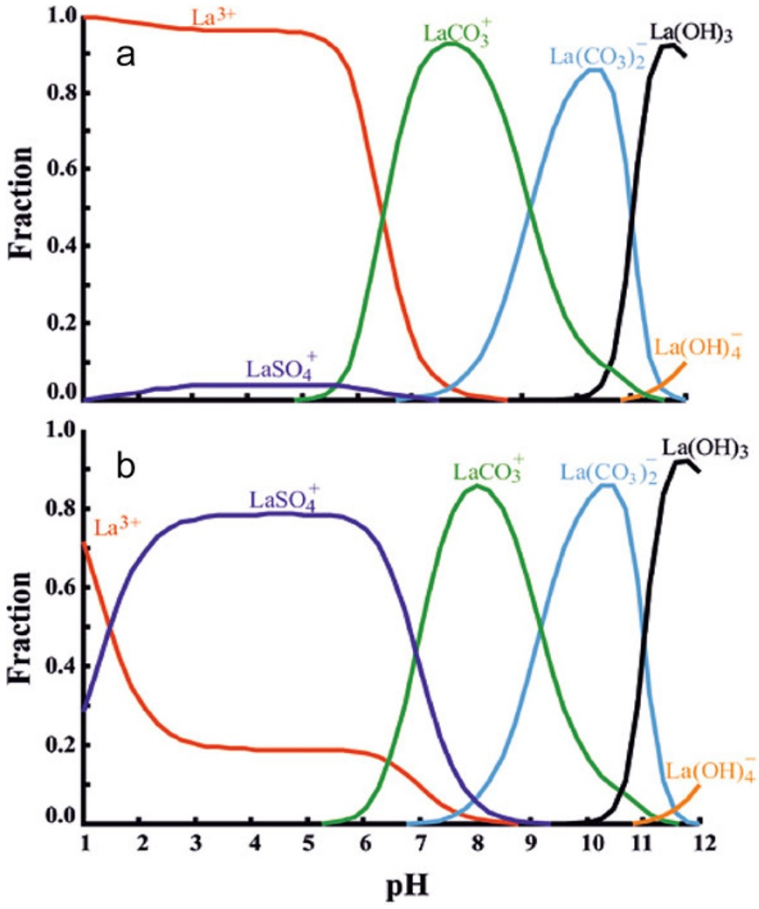


Figure 8. Proportion of the most abundant La species in solution at various pH values, corresponding to two representative fluid compositions. (a) Porewater in a common weathering profile, with 1 mM CO_3^{2-} and 0.01 mM SO_4^{2-}. (b) Fluid from an acid mine, with 0.01 mM CO_3^{2-} and 1 mM SO_4^{2-}. From Ayora *et al.* (2015).

Ligands in the fluids

As the *REE* pass into solution, their stability in the fluid depends on the species that they generate. The most abundant dissolved Ln species change with pH and anionic content (Fig. 8). Overall, the stability constants of Ln species increase in the following order: $Ln(OH)_4^- < Ln(OH)_3 < Ln(OH)_2^+ < Ln(OH)^{2+} < LnCl_2^+ < LnCl^{2+} < LnH(CO_3)^{2+} < LnF^{2+}$, $Ln(SO_4)^+ < Ln(SO_4)_2^- < Ln(CO_3)^+ < Ln(CO_3)_2^- < Ln_2(P_2O_7)^{2+}$ (neutral pH), $LnH(PO_4)^+$ (pH 4–7), $LnH_2(PO_4)^{2+}$ (pH < 4) (Brookins, 1989; Millero, 1992; Liu & Byrne, 1998). This list is not exhaustive but covers frequent species. Not surprisingly, phosphate species are very stable, in agreement with the great stability (low solubility) of phosphate Ln that causes them to concentrate *REE* and become an important industrial source of them (Chakhmouradian & Wall, 2012). Indeed, the low solubility of phosphate–*REE* phases causes waters with high phosphate contents to have low *REE* in solution due to the precipitation of *REE* phosphates (Johannesson *et al.*, 1995).

The effect of available ligands on the mobilization of *REE* is frequently directly linked to that of pH because sulfuric acid (from pyrite oxidation) is a frequent source of acidity. Thus, in Fig. 4a, low pH and high sulfate concentration are the joint causes of the high *REE* concentrations in fluids at the top (although these values are multiplied ×1000). The dark blue data points in Fig. 4a correspond to the lowest sulfate concentration of 1025 ppm, whereas the brown and green data points correspond to 1504 and 4380 ppm, respectively (Michard, 1989).

According to the order of increase in the stability constants of the various inorganic ligands referred to above (some of them represented in Fig. 8), the most abundant species in most natural waters are carbonate complexes, with one or two CO_3^{2-} groups, in neutral to moderately alkaline waters, and Ln^{3+} in acidic pH unless sulfate exceeds ~0.45 mM (for which value $[La^{3+}]_{fraction} \approx [LaSO_4^+]_{fraction} \approx 0.5$, as interpolated from Fig. 8). Although OH complexes are the weakest of all, they become abundant at very high pH due to the high OH^- concentration (Fig. 8). Phosphate is typically of low concentration due to its low abundance and to ion-pair formation with Ca and Mg so that phosphate cannot compete with carbonates at binding *REE* in solution (Johannesson *et al.*, 1996). Sulfate complexes have very similar values of stability constants for all *REE*, more so for $Ln(SO_4)^+$ than for $Ln(SO_4)_2^-$ (Brookins, 1989; Gimeno-Serrano *et al.*, 2000; Schijf & Byrne, 2004). Thus, there is no *REE* fractionation between rock and fluids where dissolution is controlled by *REE*–sulfate complexes (Gimeno-Serrano *et al.*, 2000). The *REE*–carbonate complexes, by contrast, have smoothly increasing stability constants from La to Lu and for both $Ln(CO_3)^+$ and $Ln(CO_3)_2^-$ (Millero, 1992; Liu & Byrne, 1998). Thus, there is preferential dissolution of *HREE* relative to *LREE* where *REE* speciation is carbonate-controlled. For example, at pH 9–10, where only carbonate complexes are important (Fig. 8), they constitute 86% of dissolved La and 98% of dissolved Lu (Cantrell & Byrne, 1987). The $LnH(CO_3)^{2+}$ complexes have much lower stability constants and do not compete with the two other types of carbonate complex (Millero, 1992).

Given the typical pH of natural waters (6–8; Goldstein & Jacobsen, 1988), the usual relative abundance of ligands and the relative strength of *REE*–ligand binding, carbonate ligands control dissolved *REE* in seawater and many rivers (Brookins, 1989), which

https://doi.org/10.1180/clm.2026.10030 Published online by Cambridge University Press

results in PAAS- or NASC-normalized *REE* patterns of *LREE* < *MREE* < *HREE*, following a gentle slope (Fig. 4b; Goldstein & Jacobsen, 1988). *REE* dissolved in rivers (typically with pH ≤ 8 and carbonate concentrations below those of alkaline waters; see 'Fluid pH' section above) may or may not display a negative Ce anomaly. Where there is one, it becomes more pronounced as pH increases (always below 8), perhaps due to Ce^{3+} to Ce^{4+} oxidation and removal of Ce^{4+} as oxide (Goldstein & Jacobsen, 1988). Although it is thought that the dissolution of fine sediment, which is richer in clay minerals, controls the *REE* patterns of average seawater (see above; Abbot *et al.*, 2019; Bayon *et al.*, 2023), it is of interest to point out that seawater *REE* patterns are also compatible with carbonate control of the dissolved *REE*, suggesting a possible cooperation between both mechanisms in the generation of the seawater *REE* signature.

So far, only inorganic ligands have been considered, but organic ligands can link strongly with *REE*, and, where sufficiently abundant, they are also important in controlling dissolved *REE* in natural waters. Calculated stability constants for humic and fulvic acid complexes with *REE*, the most abundant and actively complexing type of OM (Pourret *et al.*, 2007b), are in the order $LnCl_2^+ < LnCl^{2+}$, $LnH(CO_3)^{2+} <$ Ln–OM $< LnF^{2+}$, $Ln(SO_4)^+ < Ln(SO_4)_2^- < Ln(CO_3)^+ < Ln(CO_3)_2^-$ within the series provided above. Although with lower stability constants than $Ln(CO_3)^+$ and $Ln(CO_3)_2^-$, OM ligands are calculated to form complexes with greater proportions of *REE* in average river waters at circumneutral pH (Fig. 9; Tang & Johanneson, 2003; Pourret *et al.*, 2007b). The average world river water has 5 mg L^{-1} of dissolved organic carbon (Pourret *et al.*, 2007b) and ~11.5 mg L^{-1} of dissolved inorganic carbon (Tang & Johanneson, 2003). Thus, in rivers, dissolved *REE* concentrations are controlled by OM or carbonates depending on their relative concentrations, as has been found experimentally (Pourret *et al.*, 2007a). Average seawater has dissolved organic carbon concentrations ranging from ~0.45 mg L^{-1} in deep waters to ~0.78 mg L^{-1} near the surface (Sharp *et al.*, 1994), which supports the control of dissolved *REE* by carbonate ligands. Although OM has a variable *REE* signature, its PAAS-normalized *REE* pattern frequently has a gentle convex-up shape with a maximum at Eu-Gd (Pi *et al.*, 2013; Freslon *et al.*, 2014). This *REE* signature has been found in organic-rich shallow groundwaters (Gruau *et al.*, 2004) and in some rivers, such as the Amazon (Sholkovitz, 1995). The Amazon has 2.7–5.9 mg L^{-1} of dissolved organic carbon in the main river stem (Seidel *et al.*, 2016) and 5.8–12.7 mg L^{-1} of dissolved organic carbon in the main tributaries (Moreira-Turcq *et al.*, 2003). Consequently, the fact that *REE* patterns are different in lakes and rivers of different relative organic/carbonate compositions also supports the interpreted competition between organics and carbonate for binding *REE* in terrestrial waters (Fig. 9).

REE *patterns of clay minerals precipitated from fluids*

Clay minerals precipitated from solution have the *REE* signature of the solution. As discussed above, acidic and high-temperature conditions may cause differential plagioclase dissolution that modifies Eu concentrations, but as pH becomes lower and temperature becomes higher the entire rock dissolves homogeneously (there is no differential dissolution of the minerals present). At the same time, because sulfate ligands do not fractionate *REE*, neoformed clay minerals precipitated from such solutions preserve the *REE* signature from the original rock that was dissolved, although at lower concentration. Alkaline, carbonate-rich waters, however, are consistent in generating a *REE* pattern of *LREE* < *MREE* < *HREE*, following the selectivity order of carbonate anions. The exception may be waters with very abundant OM, where this OM may perceptibly modify the *REE* signature given by dissolved carbonate. If clay mineral precipitation from alkaline water is massive or, at any rate, generates a significative part of the deposited clay minerals (with respect to detrital clay minerals), the *REE* signature of the precipitated clay minerals will modify that of the detrital phyllosilicates.

Such is possibly the case in the following example. The *REE* patterns (normalized to upper-crust composition) of clay mineral-bearing sediments in alkaline lakes ($Ca–HCO_3–SO_4$ waters) of pH 9.0–10.4 were found to be slightly enriched in *LREE* over *HREE* (Volkova, 1998). This pattern is the inverse of the typical *REE* concentration in alkaline waters (Fig. 7) and suggests incomplete control of the *REE* sediment composition by the waters *via* carbonate complexation. The greater control on the *REE* signature was most probably generated by the detrital sediment (mineral and organic), given that *REE* concentrations in sediments are much higher than in waters and cannot be easily influenced by newly precipitating minerals.

REE *pattern modifications in low-temperature alteration processes*

Clay minerals are typical and abundant products of low-temperature alteration. They are especially abundant from the alteration of volcanic materials, which are rich in amorphous constituents and labile minerals. Most times, clay mineral products of volcanic ash alteration preserve the *REE* signature and concentration of the ash (Karakaya *et al.*, 2001; Namayandeh *et al.*, 2020; Šegvić *et al.*, 2024). Modifications, however, occur depending on the specific conditions of alteration, which may increase or decrease total *REE* concentration and change the behaviour of Ce and Eu following variations in oxygen fugacity (Ce, Eu) and differential alteration (Eu), most particularly of plagioclase (Karakaya *et al.*, 2001; Namayandeh *et al.*, 2020; Šegvić *et al.*, 2024).

Bentonites are phyllosilicate-rich products of alteration of pyroclastic rocks in a variety of environments. Although the *REE* content may vary widely, the most abundant values are in the range 250–300 ppm (e.g. Christidis, 1998; Kiipli *et al.*, 2017; Fontain *et al.*, 2020). Bentonites are richer in *LREE* relative to *HREE*, displaying chondrite-normalized patterns with steeply decreasing values in the *LREE* section, negative Eu anomalies and a *HREE* section ranging from flat in felsic bentonites to gently decreasing in bentonites deriving from basic rocks (Fontaine *et al.*, 2020; Namayandeh *et al.*, 2020). The negative Eu anomaly is most probably due to plagioclase fractionation, as is to be expected from evolved magmas originating from the crust, or to preferential plagioclase alteration. This pattern is preserved from their precursors and is controlled by Ln contraction. As *REE* become smaller from *LREE* to *HREE*, they become more compatible (with silicates) and less abundant in evolved melts. Detail modifications are produced by diverse factors, such as high oxygen fugacity causing Ce oxidation and Ce negative anomalies (Chakhmouradian & Wall, 2012).

Because the above *REE* patterns are similar to those found in monazite, apatite and bastnäsite minerals (Chakhmouradian & Wall, 2012; Benson & Watts, 2024), the question is raised as to how much of their concentration in bentonites is controlled by phosphates. In fact, monazite has been reported as the main *REE* host in some bentonites (Christidis, 1998). In addition, *REE*-host phosphates may not only be present in the deposited pyroclastics but also be formed during the bentonitization process

https://doi.org/10.1180/clm.2026.10030 Published online by Cambridge University Press

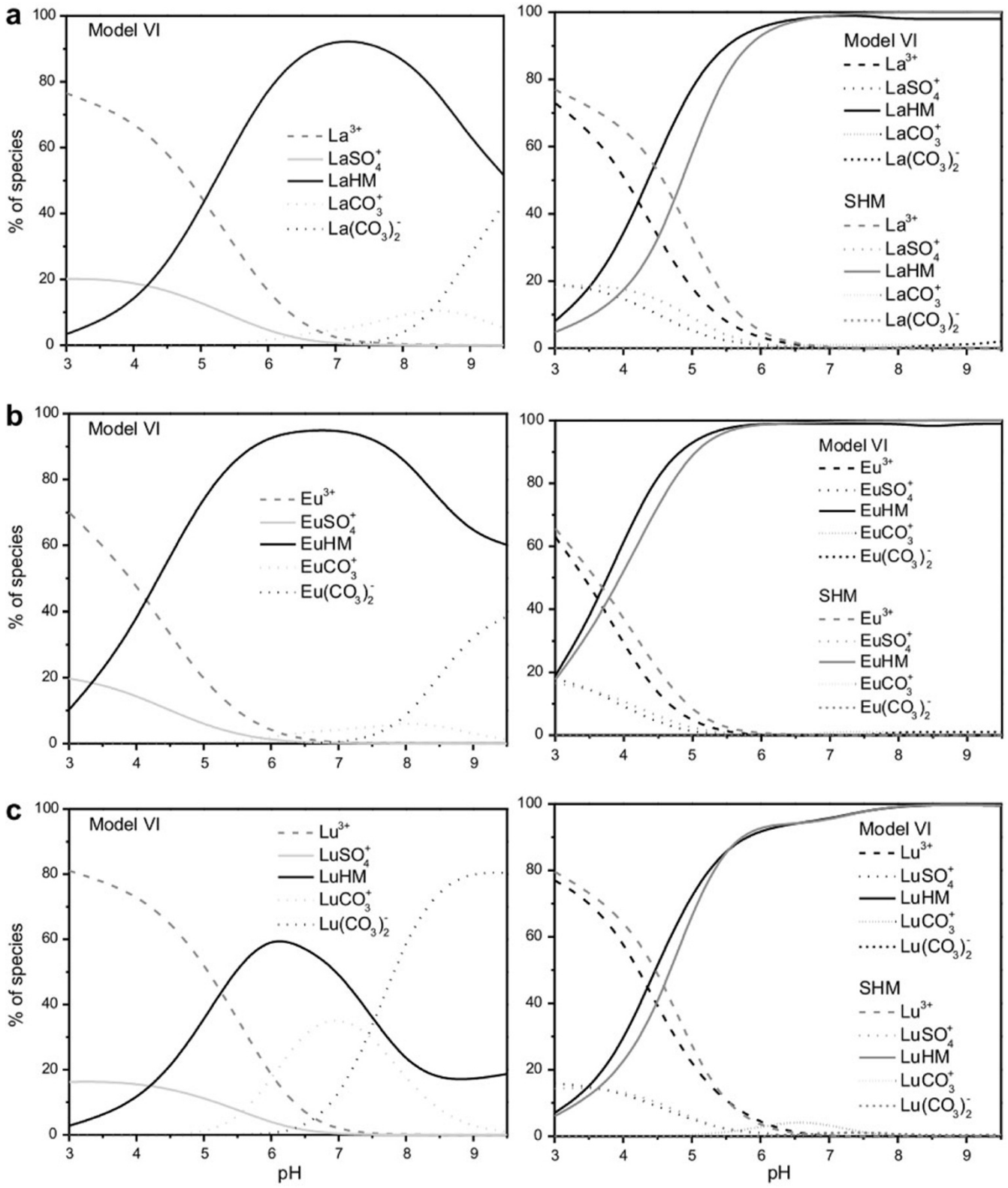


Figure 9. Assessment of the relative proportions of dissolved species of (a) La, (b) Eu and (c) Lu in world river average water (Pourret *et al.*, 2007b). The values are modeled using Model VI and the Stockholm Humic Model (SHM). LnHM is *REE* bound to OM. For the graphs on the left, the 'active dissolved OM parameter' (OM capable of complexing *REE*) within the models is 50%; for the graphs on the right, this parameter is 100%. The results of SHM for the left-hand column series (not shown) are similar to those of Model VI, with slightly lower percentage values of LnHM.

https://doi.org/10.1180/clm.2026.10030 Published online by Cambridge University Press

(Berti *et al.*, 2022). The mobility of *REE* during the bentonitization process and later depends on their hosts, increasing from primary or secondary phosphates to silicate glass and minerals. However, as mentioned above, bentonites typically preserve the *REE* signature from their precursors (Kiipli *et al.*, 2017).

A slight *REE* fractionation is sometimes described where bentonite formation causes a relative decrease in *HREE*. This fractionation is contrary to the intrinsic *REE* mobility, which is lower for *HREE* due to their higher electric charge-to-radius ratio. Thus, the fractionation is ascribed to the presence of phosphates, which retain *LREE* preferentially. Christidis (1998) showed plots of *REE vs* Al_2O_3 concentrations for several Greek bentonites and their protoliths, where Al_2O_3 represents an immobile cation. These plots displayed deviations from the trendlines of *REE vs* Al_2O_3 of the protoliths. *LREE* displayed only a slight deviation that indicated mild mobility of *LREE* during bentonitization. The deviation increases in the same direction for *MREE* and is most pronounced for *HREE*, indicating increasing depletion.

REE *pattern modifications in soils*

Pedogenic processes typically concentrate *REE* in soils relative to parent rock up to a factor of two (McLennan, 1989) – and even up to a factor of seven (Duddy, 1980) – due to the loss of material during weathering, at the same time that *REE* are concentrated in clay minerals, which have the greatest retention capability among silicates, and in Fe-Mn nodules (Xin & Dudas, 1993; Ramos *et al.*, 2016). In other cases, however, *REE* concentrations in soils are reduced with respect to the protolith, as in acidic pedogenic alteration, where the transport of dissolved *REE* is more efficient and the formation of secondary phases is less so (Fernández-Caliani, 2018).

Across soil profiles, pedogenesis causes a dilution of *REE* in top horizons and a concentration of *REE* in bottom horizons. Such an effect is due to eluviation (transport of fines down the soil profile), because *REE* are preferentially retained in the fine fractions (McLennan, 1989; Aide & Aide, 2012; Cidu *et al.*, 2013). However, OM also retains *REE* effectively and typically decreases with soil depth (Spain *et al.*, 1983). Therefore, organic-rich soils can have a more homogeneous distribution of *REE* with depth, although the *REE* signatures at the top (controlled by organics) and at the bottom of the profile (controlled by phyllosilicates) are typically different. Podzols are an exception where the abundant OM complexes with metals, including *REE*, and migrates to the lowest illuviated horizon (Laveuf & Cornu, 2009). The usual sandy texture of podzols facilitates the downward migration of organics, with their load of *REE*, while at the same time clay minerals are not abundant and so have little role in *REE* distribution. Slopes have a similar effect as soil depth, causing an increased *REE* concentration at the bottom of a slope (Cascante *et al.*, 2025).

With respect to fractionation, *REE* preferential retention in clay minerals most frequently causes concentration of *HREE* in bottom soil horizons (Aide & Aide, 2012; Cidu *et al.*, 2013), although sometimes it is *LREE* that concentrate in lower horizons (Aide & Aide, 2012). These differences are due to the wide range of possibilities of soil mineral composition and chemistry together with the extent of weathering (Laveuf & Cornu, 2009).

Extensive weathering in both rock and soils is frequently characterized by the weathered material having *LREE* > *HREE*. Such is the case in 'white clay soils' (i.e. kaolinite-rich soils; Xing & Dudas, 1993). Galán *et al.* (2007) investigated the kaolinization of alkaline peraluminous granitoids containing apatite and zircon at various depths within the deeply altered rock. At 3–15 m depths, *REE* concentrations in kaolinite were higher than in the granitoids and displayed *LREE* > *HREE* ($La_N/Sm_N = 1.22–2.53$). At 12–21 m depths, *REE* concentrations were the same as in the granitoid, excepting more marked positive or negative Eu anomalies in the altered rock. Similarly, Silva *et al.* (2017, 2018) reported that kaolinite in Brazilian soils derived from meta- and per-aluminous granites concentrated *REE* and developed *REE* patterns with a down slope from *LREE* to *HREE* that correlated with the Chemical Index of Alteration (CIA). Although these granites contained apatite and monazite, kaolinite displayed stronger mineralogical correlations with *REE* than the phosphates. Accordingly, the higher relative concentration of *LREE* in kaolinite may be due to late breakdown of *REE*-bearing accessory minerals and their adsorption on kaolinite. Because apatite and monazite greatly concentrate *LREE* over *HREE* (Mariano, 1989), their dissolution would release *REE* with the profile *LREE* ≫ *HREE*. The combined loss of material due to alteration and the dissolution of *REE*-bearing trace minerals generated the apparent correlation between *LREE* and kaolinite, although, intrinsically, kaolinite retains *HREE* preferentially, as in all other clay minerals.

Redox changes in soils concern only Ce, which can be oxidized by Mn reduction and precipitate as cerianite, CeO_2, with Mn oxides (Laveuf & Cornu, 2009). Cerianite is thus typically enriched in soils with Mn oxides, which develop the corresponding Ce positive anomaly. The great stability of cerianite (Brookins, 1989) causes it to remain in the soil even if Mn oxides are removed (Laveuf & Cornu, 2009).

REE *pattern modifications in burial diagenesis*

Given the conservative behaviour of *REE* in phyllosilicates, little or no changes are expected in the *REE* distribution in shales during their diagenetic transformations. Such was the conclusion of Condie (1991) in his global analysis of cratonic shales, in which he found clay minerals to be the most important mineral group controlling *REE* distribution. Indeed, this is one of the reasons why average shales are good representatives of the *REE* composition of the surface siliciclastic materials.

However, *REE* average values are not identical to those of individual shales. Pipe *et al.* (2025) investigated black shales from north-east North America with different degrees of thermal maturation: immature (maximum temperature 20–50°C), mature oil-bearing (maximum temperature = 50–140°C) and post-mature gas-bearing (maximum temperature >200°C). When normalized to PAAS, all shales had an approximately flat *REE* distribution, with normalized values ranging from ~0.4 to ~1.0 for the immature and mature shales and from ~1.0 to ~1.5 for the post-mature shales, with the average values increasing from immature to post-mature. Supposedly, the range of compositions of immature and mature shales was caused by the several origins of their clay minerals (two locations sampled for the immature shales and three locations sampled for the mature ones), while the increasing average *REE* concentrations were caused by diagenesis. However, an earlier study of Abanda & Hannigan (2006) on the same samples produced the lowest *REE* content for the post-mature shales. Pipe *et al.* (2025) also separated the *REE* contribution of labile minerals (major and minor carbonates, minor sulfides, oxides and phosphates) and OM. These fractions had a similar range of normalized *REE* concentrations as indicated above but a different pattern, with *MREE* higher than *LREE* and *HREE*. The authors concluded that all *REE* were

https://doi.org/10.1180/clm.2026.10030 Published online by Cambridge University Press

derived from the terrigenous sediments, mainly from the phyllosilicates, and that the *MREE* enrichment in the labile fractions was due to preferential loss of *LREE* and *HREE* during diagenesis. Overall, although the authors refer to significant changes to the *REE* distribution with shale maturation, we observe that: (1) the *REE* composition was controlled by the phyllosilicates, not by the labile minerals; (2) the apparent modification produced by diagenesis is in the range of composition of individual shales; and (3) only one location of post-mature shales was sampled by Pipe *et al.* (2025), with their results contrasting with those of Abanda & Hannigan (2006), all of which weakens the interpretation that *REE* concentration grew uniformly with maturity. The phyllosilicate composition of the shales consisted of muscovite (4–47 wt.%) and clinochlore (1–12 wt.%; Pipe *et al.*, 2025).

Importantly, shales contain OM, which in the case of black shales may retain ∼20% of the total *REE* content (Abanda & Hannigan, 2006). OM may have several effects. First, it promotes reducing conditions during burial and the possibility of Eu reduction to Eu^{2+}, which may result in its selective loss to solution. Second, OM transformations modify reactivity with both minerals and *REE*. For example, low-molecular-weight organic acids produced during diagenesis can both dissolve minerals and act as efficient ligands of *REE*, possibly causing *REE* signature modifications (Kawamura & Kaplan, 1987). At the same time, however, the low permeability of shales hinders fluid mobility and *REE* loss. Experiments have observed that *REE* released by OM are retained in shales (Nakada *et al.*, 2016). Over the long term, even if the condensation of OM and the formation of kerogen and methane may modify the *REE* signature of OM (Zhao *et al.*, 2023), adsorption by phyllosilicates appears to preserve the *REE* distribution in the rock.

Sandstones have lower *REE* concentrations due to their lower clay mineral content (Cullers, 1995; van de Kamp, 2019). Supposedly, their greater porosity may facilitate *REE* reactivity and loss, although this may be balanced if the entire rock dissolves in the same proportion, preserving the *REE* concentration. In his study, van de Kamp (2019) found that the average *REE* concentrations in Ordovician shales and sandstones from Oklahoma and Kansas reproduced those of the original rocks and showed no diagenetic modifications.

Krull-Davatzes *et al.* (2012) conducted a very interesting study of the mineralogical and geochemical modifications of spherules from a very ancient meteorite impact (3.24 Gyr) through diagenesis and lower greenschist grade metamorphism. The initial glass spherules were palagonitized, became cemented by silica and later transformed into quartz, phyllosilicates and feldspar assemblages. The original phyllosilicate was smectite, which was later transformed into sericite and chlorite. Spherule morphology was preserved during all of these events. *REE* displayed individual variations, which were larger in *LREE*, but their averages by locality were all within a narrow range, with a gentle decrease of *REE*/chondrite values from *LREE* to *HREE*. The higher *LREE* concentrations were related to diagenetic carbonatization and phosphate authigenesis rather than being related to modifications within silicates (Krull-Davatzes *et al.*, 2012). This investigation shows that phyllosilicates can preserve their *REE* signature for very long periods of time and throughout significant environmental changes (late peak metamorphic temperatures were 300–320°C).

REE *pattern modifications in ore deposits*

This section refers to ore deposits where phyllosilicates play a role, and it focuses on their contribution to the overall *REE* signature. Modification of the *REE* distribution in ore deposits is controlled by the mechanisms that generated the ore enrichment. Such mechanisms have been discussed above, and this section briefly summarizes the modifications that take place and their causes.

Sometimes, lateritic-type deposits generated by extreme weathering develop at near-neutral conditions due to protolith composition (e.g. argillaceous limestone) or due to the influence of nearby carbonates. In such cases of near-neutral weathering, *REE* are enriched with little fractionation. This is well-exemplified by a bauxite deposit in Iran displaying Σ*REE* 4–17 times greater than that of the original rock, with low fractionation (Ahmadnejad *et al.*, 2017). The mineralogy of the deposit consisted of metal oxides and hydroxides, with chlorite being the only clay mineral present only as a minor component. The increased concentration was due to the loss of material during weathering while *REE* were retained by the oxides, which have similar *REE*-related characteristics to clay minerals (i.e. good retention and little segregation of *REE*). In most cases, however, laterite formation environments are acidic and greater *REE* mobility takes place, by which *REE* are partially lost from the laterite, and those remaining are retained by metal oxides and hydroxides as well as by minor kaolinite.

REE in hydrothermal ore deposits undergo modifications controlled by the temperature and pressure of the hydrothermal fluid, the fluid/rock ratio, the pH and Eh conditions of the fluids and ligand type and concentration (Lottermoser, 1992; Fulignati *et al.*, 1999). Phyllosilicates retain a high proportion of the *REE* in the original silicate rocks without substantially changing their relative concentrations, especially in low water/rock conditions (Parsapoor *et al.*, 2009; Cuadros *et al.*, 2023). However, low- to mid-temperature hydrothermal fluids dissolve plagioclase preferentially to other silicates and thus also preferentially mobilize Eu. Thus, secondary clay minerals forming from the interaction of such fluids and plagioclase-rich rock incorporate a significant positive Eu anomaly (Fig. 4; Shikazono *et al.*, 2008). A striking example of this effect is the *REE* composition of interstratified chlorite-smectite precipitated from the alteration of corrensite-rich sediments in a hydrothermal deposit of the Juan de Fuca ridge (Fig. 10). In addition, clay mineral interaction with and precipitation from hydrothermal fluids charged with ligands may also modify the *REE* signature of the clay minerals.

In ores generated by acidic alteration at surface temperatures there are two main variables controlling *REE* mobility and fractionation: fluid pH and sulfate concentration. Fluid pH values below ∼5 are at the threshold of becoming sufficiently acidic to cause bulk dissolution of silicate rocks, while the sulfate concentration in the fluid is high enough to compete efficiently with solid phases for the retention of *REE* (Verplanck *et al.*, 2004; Cuadros *et al.*, 2023). At this pH, kaolinite and alunite may coexist, which marks the transition from silicates to sulfates as secondary minerals at equilibrium with the altering solutions (Mavris *et al.*, 2018). This factor can greatly modify *REE* of the rock at pH < 5 because (1) sulfate minerals greatly segregate *REE* (Martínez *et al.*, 2007; Parsapoor *et al.*, 2009; Welch *et al.*, 2009; Kikawada *et al.*, 2013; Dutrizac, 2017) and (2) the increasing extent of rock dissolution makes possible large rock and *REE* losses, which may result either in *REE* dilution or concentration in the secondary mineral assemblages (Cuadros *et al.*, 2023). However, for pH < 3, with precipitation of jarosite-group minerals, there are also reports of the altered rock preserving the *REE* patterns of the precursor (Pérez-López *et al.*, 2010; Romero *et al.*, 2010; Mitra *et al.*, 2017). This discrepancy requires further investigation.

https://doi.org/10.1180/clm.2026.10030 Published online by Cambridge University Press

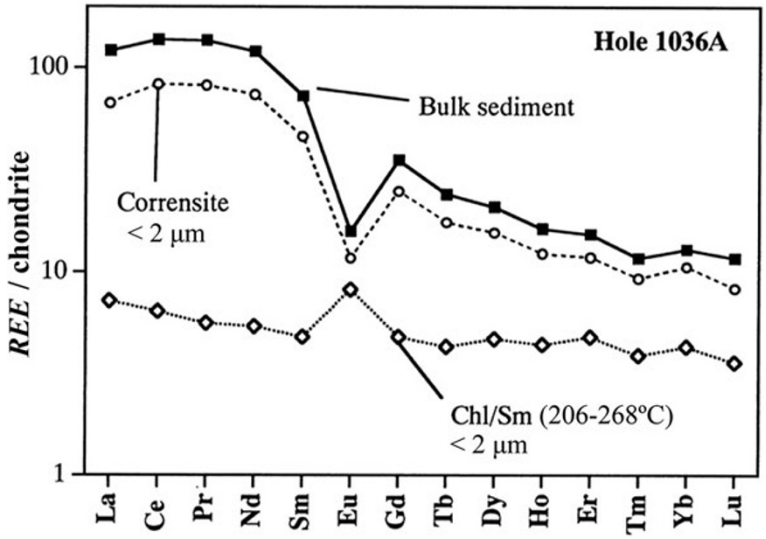


Figure 10. *REE* compositions of bulk precursor sediment, corrensite (<2 μm) from the same sediment and chlorite-smectite (Chl–Sm; <2 μm), a product of hydrothermal alteration of the sediment at 206–268°C. Hydrothermal fluids selectively dissolved plagioclase, which caused Eu to dissolve preferentially to other *REE*, and the newly formed Chl–Sm inherited the corresponding *REE* signature from the fluid. Figure modified from Lackschewitz *et al.* (2000).

REE pattern modifications during transport

River transport

For this section, it is useful to appreciate the difference between UCC- and PAAS-normalized REE. In both cases, river sediments generally produce *REE* patterns decreasing from *LREE* to *HREE*, but these are not exactly coincident (Fig. 11). Most importantly, the ratio REE_{UCC}/REE_{PAAS} produces a high value for Lu, an element frequently used to calculate *LREE*/*HREE* ratios, which means that such a ratio appears higher for PAAS-normalized values than for UCC-normalized *REE*. This and other differences between normalized *REE* compositions need to be considered when comparing the results from different studies.

Because solid phases contain *REE* concentrations orders of magnitude larger than those dissolved in seawater and most natural freshwaters (Fig. 2a; Taylor & McLennan, 1985; Brookins, 1989), and because clay minerals hold the highest *REE* concentrations of all abundant minerals on the surface of the crust (phosphates and metal oxide phases are less abundant than clay minerals), *REE* pattern modifications by water transport are generally those produced to clay minerals. The exceptions are terrestrial waters with very abundant OM, which may contribute a substantial proportion of *REE*. The main expected effect of water transport on sediments is particle sorting by size. Because clay minerals are concentrated in the finer fractions, which are more easily water-borne, river transport could produce *REE* concentrations in the suspended and deposited sediment along the river, but the new sediments sourced at every stage reduce this clay mineral concentration effect. The study of Bayon *et al.* (2015) already presented (see the 'Influence of phyllosilicates on the concentration and distribution of *REE* in rock, sediment and soil' section above) is relevant here. These authors found that, globally, silt in river sediments represents very closely the average upper-crust *REE* composition, while clay-size sediments have a slightly higher *LREE* concentration. Similarly, global average suspended loads (i.e. fine fraction >0.2 μm) have been found to be enriched in *LREE* (La/Yb ≈ 1.9 for NASC-normalized values; Goldstein & Jacobsen, 1988), as was the case with suspended sediments from several rivers in south-east China (typical values of La/Yb ≈ 1.5 as normalized to PAAS), with a substantial positive Gd anomaly of anthropological origin in the latter (Liu & Han, 2021). The suspended sediments in these Chinese rivers were enriched in total *REE* by 1.5–2.0 times with respect to PAAS (Liu & Han, 2021). Greater *LREE* enrichment (La/Lu = 5; values normalized to European shale) was found in the Miño river (north-west Spain; Álvarez-Vázquez *et al.*, 2022). In contrast, the sediments <63 μm in size from Taiwan rivers displayed UCC-normalized *REE* concentrations that were very slightly enriched in *MREE* (Sm to Dy), and their average *REE* concentrations were 1.0–1.8 times those of the UCC values (Li *et al.*, 2013). One more global study of river-suspended particles (<0.45 μm) by Elderfield *et al.* (1990) found that shale-normalized patterns of *REE* were slightly below 1 and had an average La/Lu ratio of 0.9 (i.e. slight enrichment of *HREE*). Such *REE* concentrations were independent of the lithology traversed by the rivers (Elderfield *et al.*, 1990). In a study of five rivers from Korea and north-east China, UCC-normalized *REE* values of bulk sediments were 1.0–1.6 and La/Yb values were between 1.39 and 0.99 (Xu *et al.*, 2009). *REE* patterns showed some consistent small variations between Korean and Chinese rivers, linked to source compositions (Xu *et al.*, 2009).

Su *et al.* (2017) investigated three rivers in south-east China (subtropical humid climate) and found that both sediments and suspended material had UCC-normalized *LREE*/*HREE* ratios of between 0.5 and 1.0. The slight (on average) enrichment of *HREE* with respect to *LREE* was attributed to the increased fine-to-coarse particle ratio in the river load with respect to the average upper crust. Su *et al.* (2017) also found that *LREE*/*HREE* ratios in weathered profiles near the rivers ranged from 0.2 to 0.8. The comparison between the two ranges of values indicates that the effect of clay mineral concentration (i.e. to decrease the *LREE*/*HREE* ratio) produced by weathering (*LREE*/*HREE* = 0.2–0.8) was reduced by river transport (*LREE*/*HREE* = 0.5–1.0). The reason for this modification may be that proposed by Bayon *et al.* (2015): that plagioclase alteration produces very fine phyllosilicates with *LREE* > *HREE*, which is selectively washed into river systems (rather than remaining in weathered profiles). The total concentration of *REE* found by Su *et al.* (2017) in river samples was mainly within the range of the sources, with a few samples reaching up to approximately twice that value. Overall, this study showed absolute *REE* concentrations not to be significantly modified in river sediment loads, while the *REE* patterns had slightly lower *LREE*/*HREE* values than

https://doi.org/10.1180/clm.2026.10030 Published online by Cambridge University Press

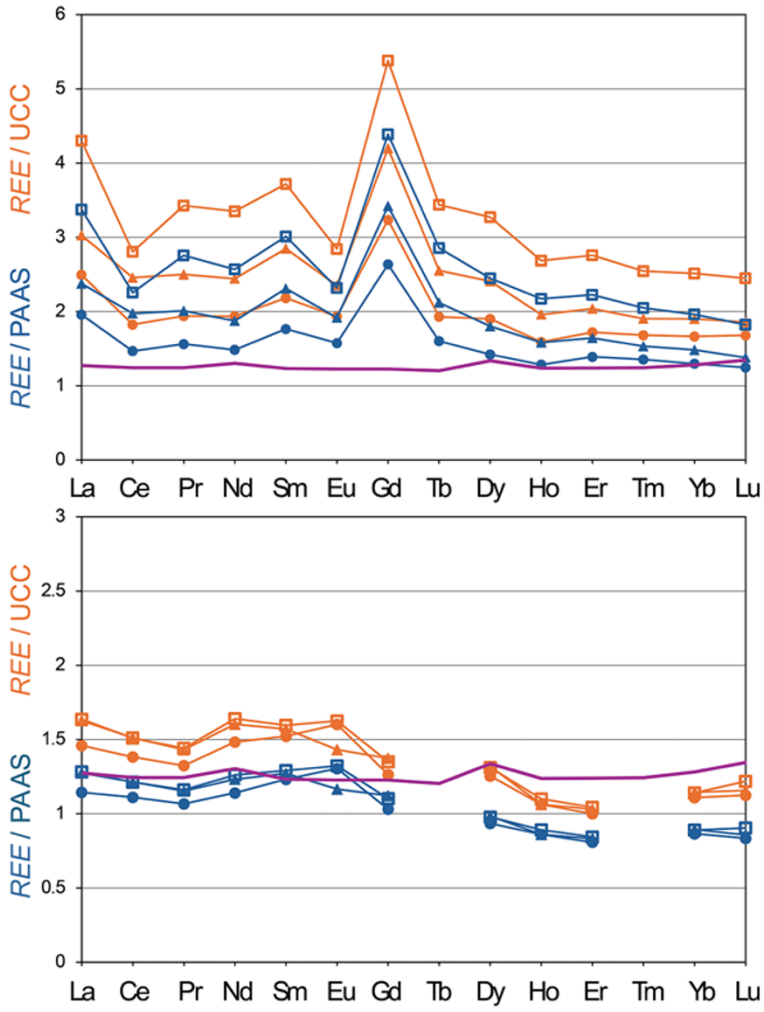


Figure 11. The concentrations of *REE* in river sediments from Liu & Han (2021) and Xu *et al.* (2009), both corresponding to south-east China, are shown as normalized to UCC and PAAS. Both display a relative enrichment of *LREE*, but the ratio between UCC- and PAAS-normalized values (purple line) is not constant, which is particularly important for La and Lu – elements that are frequently used to calculate *LREE*/*HREE* as La/Lu.

the average crust but higher *LREE*/*HREE* values than weathered profiles along the course of the rivers.

In summary, *REE* in rivers are controlled by clay minerals in particulate matter. The concentration of *REE* in this particulate matter is typically similar to but higher than in the UCC and closer to shale *REE* standards because the latter correspond to weathered material. The corresponding *REE* patterns are approximately flat or with small slopes. The *REE* concentration in river sediments and suspended particles is near or slightly higher than in the surrounding soils. There is no apparent modification of *REE* concentration or pattern along the rivers. The most important *REE* variations are produced by particle segregation. Coarse fractions from soils, which have low *REE* abundance, reach rivers in small proportions. Silt fractions are enriched in the riverbed sediments. Silts have the most similar *REE* contents to soils in surrounding areas and even to UCC, although they may display enrichment in *HREE*, interpreted as resulting from the control by phyllosilicates (which have greater affinity for *HREE*). The clay fraction is more abundant in suspension. Clay fractions most frequently display enrichment of *LREE*, possibly due to plagioclase alteration generating fine clay mineral particles, although this mechanism acts in opposition to the enrichment of *HREE* produced by adsorption on phyllosilicates. In consequence, the *REE* patterns of clay fractions in rivers are sometimes enriched in *HREE*, supposedly depending on the concentration of plagioclase in the several sediment sources.

Transport in estuaries and seas

The entry of river water into estuaries immediately produces a decrease of *REE* content in suspended sediments. Two reasons for this have been proposed. First, *REE* are desorbed from clay minerals due to the higher cation concentration in solution and thus the more effective competition for adsorption sites in the suspended sediments (Liu & Han, 2021). Because *HREE* are most strongly adsorbed onto clay minerals, *LREE* desorb preferentially, and increasingly more so as ionic strength increases (Coppin *et al.*, 2002). The reported average *REE* losses from suspended sediments in three Chinese rivers ending in the same estuary are ~100 mg kg^{-1} for *LREE*, <10 mg kg^{-1} for *MREE* and <5 mg kg^{-1} for *HREE* (Liu & Han, 2021). The second reason for decreased *REE* content in suspended sediments is the flocculation and sedimentation of *REE*-bearing particles, such as clay minerals, Fe oxides and OM (Edzwald & O'Melia, 1975; Elderfield *et al.*, 1990; Sholkovitz, 1993; Pourret & Tuduri, 2017; Arienzo *et al.*, 2022; Febina & Priya, 2024). Both effects – desorption of *REE* from particles and particle flocculation – increase with water salinity.

https://doi.org/10.1180/clm.2026.10030 Published online by Cambridge University Press

Thus, *REE* concentration in both suspended and flocculated sediments decreases and becomes *HREE*-enriched relative to *LREE*. The result in the water, which comprises fine suspended matter together with dissolved *REE*, is more complex. There is *REE* loss due to flocculation (Elderfield *et al.*, 1990), some relative enrichment of *LREE* due to desorption from the solids and modification due to the simple mixing of the waters, because the patterns of dissolved *REE* and *REE* in suspended particles in rivers (entering the estuaries) are different. In particular, Elderfield *et al.* (1990) found that the patterns of dissolved *REE* in rivers was enriched in *HREE*, while the suspended fraction had a flatter, shale-like pattern. Thus, flocculation of suspended particles reinforced the *HREE*-relative enrichment in the waters produced by salt displacement of *REE* from particles. However, flocculation produces the greater effect of the two mechanisms due to the low dissolved amounts of *REE*.

Moving further into the ocean, particle precipitation progresses. The water column receives the input of wind-transported dust, where sorting of airborne mineral particles means that the input is reduced farther away from the continent and consists of smaller, more reactive particles (Chamley, 1989). Processes similar to those in estuaries continue further into the ocean but at a lesser scale, with relatively less dust deposition and particle flocculation and relatively more *REE* dissolution or desorption (Greaves *et al.*, 1999). Far from land, *REE* in seawater are most probably controlled by carbonate ligands (Brookins, 1989) and clay mineral dissolution and authigenesis in sediments (Abbot *et al.*, 2019). The *REE* signature of open ocean water relative to the upper-crust average displays a trend of constantly increasing concentration from *LREE* to *HREE* with a strong Ce negative anomaly (Fig. 4b), the latter being due to oxidation to Ce^{4+} and precipitation as oxide (Goldstein & Jacobsen, 1988). In particular, sea-floor Fe-Mn nodules are rich in Ce (McLennan, 1989; Dubinin & Sval'nov, 2003). The bulk of detrital phyllosilicate-rich sediments in estuaries and the deep sea retain their signature *LREE* < *MREE* < *HREE* (Qiu *et al.*, 2022b), and, in estuaries, they are most often depleted in total *REE* with respect to river sediments due to removal by salinity (Babu *et al.*, 2021).

Aeolian transport

The quantitative importance of aeolian transport and deposition has been recognized. Early modelling of dust mobilized from Africa and deposited between the 15°N and 24°N parallels indicated ~260 Mtons $year^{-1}$ transported westward, with ~128 Mtons $year^{-1}$ sedimented in the first 1000 km, ~22 Mtons $year^{-1}$ sedimented in the next 1000 km (2000 km from the coast) and ~11 Mtons $year^{-1}$ sedimented from 2000 to 5000 km, with ~50 Mtons $year^{-1}$ still travelling west at 5000 km from the coast (Chamley, 1989). Lawrence & Neff (2009) calculated that the global background dust deposition is in the order of 0.05–1.00 g m^{-2} $year^{-1}$.

Similar principles apply to the airborne transport of clay minerals with respect to river-borne transport, with the main (but not only) difference being that the lower density of air accentuates differential settling. Particles in the range 5–50 μm are transported from a few to ~100 km, thus mainly within the continents, and reaching the sea only if dust sources are near the coasts. Particles 2–10 μm, with most <5 μm, can be injected into the troposphere, where they can travel up to thousands of kilometres as aerosols and are brought back down by rainfall (Chamley, 1989). Recently, a modal particle size decrease from 32 to 4 μm was recorded in five submarine traps across the Atlantic, at 12°N, from the Sahara to America (van der Does *et al.*, 2016). Smaller particles are more phyllosilicate-rich (Feng *et al.*, 2011) and, in the absence of minerals that greatly concentrate *REE* (e.g. phosphates, zircon), have greater *REE* concentration. Ferrat *et al.* (2011) reported reductions of 1.5–3.0 in *REE*/UCC ratios in particle sizes from <4 to >63 μm. However, Feng *et al.* (2011) found similar total *REE*/PAAS ratios from <2 to 32 μm and only a small reduction of ~1.2 for >50 μm, although the main decrease was that of *HREE*, which preferentially concentrate in clay minerals. Because there is no or weak interaction of the airborne phyllosilicates with the transport medium (water is in low concentration in air), the *REE* signature of the clay fraction is preserved (Ferrat *et al.*, 2011). Furthermore, even if *REE* patterns are particle size-dependent, certain ratios between various *REE* are not (Nakai *et al.*, 1993; Ferrat *et al.*, 2011).

REE in phyllosilicates as tracers of geological processes and precursors

Geochemists have long pursued the goal of using *REE* signatures to trace the origins of rocks and sediments as well as their geological histories. Given the large number of factors that affect such signatures, this goal is made increasingly difficult as the history of the rock or sediment becomes more complex. Even so, the advancing understanding of how specific processes that affect *REE* dissolution, complexation and retention by solids and colloids and the resulting segregation is providing an ever-increasing capacity to trace back the processes that operated and the type of parent rock. In this exercise, *REE* data complement and support primary geological and geochemical evidence and discriminate between the several possibilities consistent with such primary evidence. Phyllosilicates are useful *REE* tracers because they are ubiquitous, concentrate *REE*, are sufficiently stable to be a lasting *REE* record and either preserve the *REE* signature from their precursors or have it modified according to known patterns. The ideal approach would be to also learn about and use the responses of a range of other minerals (oxides, sulfates, carbonates, salts and, most importantly, phosphates) to geological processes and to be able to analyse *REE* in each mineral separately. This strategy would produce a self-constraining *REE* dataset allowing very robust interpretations. In the following, we offer examples illustrating how the principles

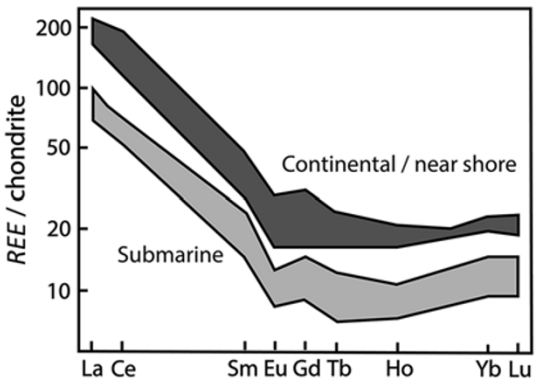


Figure 12. *REE* composition range (relative to chondrites) of Permian shales from the Havensville and Eskridge formations in Kansas and Oklahoma. The Oklahoma sediments (dark grey) are interpreted as having been deposited in continental or near-shore oceanic environment, while those from Kansas (light grey) are interpreted as having been deposited in a submarine environment. Submarine shales have lower total *REE* concentrations and higher *HREE*/*LREE* values (Cullers *et al.*, 1975).

https://doi.org/10.1180/clm.2026.10030 Published online by Cambridge University Press

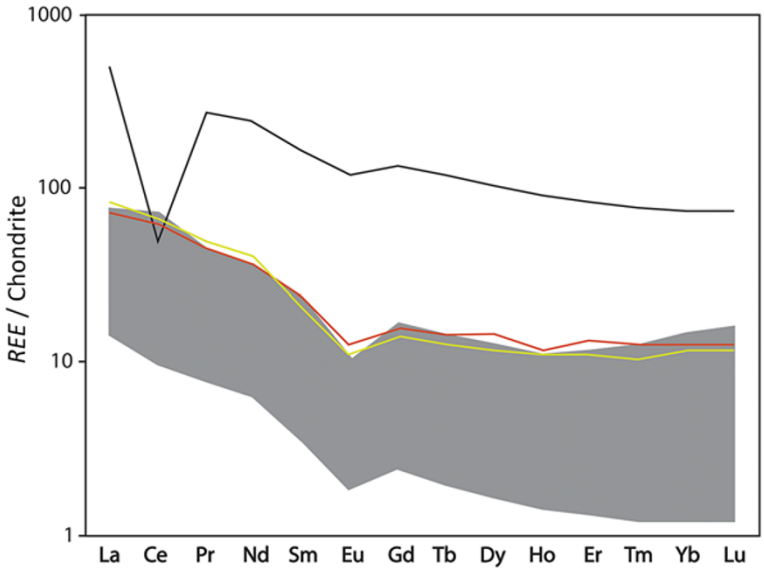


Figure 13. *REE* distribution in the Brazilian shales and claystones of the Permian Irati formation, Paraná Basin (grey contour and black line). All but the one represented by the black line are below world-average values for shales: red and yellow lines are NASC and PAAS values, respectively. The one claystone above the averages and with a large negative Ce anomaly is interpreted as having a different precursor (see text). Data from Dos Anjos *et al.* (2010).

described in previous sections for phyllosilicates have been used in this respect.

Sedimentary processes

An early example of the use of *REE* to trace geological sedimentary processes was that of Cullers *et al.* (1975). They investigated the clay fraction of Lower Permian shales from the Havensville and Eskridge formations across northern Kansas and northern Oklahoma. They found that the *REE* of the clay fraction was not controlled by clay mineralogy, although different phyllosilicates had different *REE* patterns and the relative proportions of clay minerals varied across samples. Rather, *REE* patterns changed uniformly from north to south. Cullers *et al.* (1975) concluded that the shales had a substantially unique origin of an igneous nature recognizable in the *REE* patterns (Fig. 12). Northen Oklahoma shales, with a *REE* signature closer to that of the igneous source, were interpreted to have been deposited in continental or near-shore environments, where *REE* remained unmodified. Northern Kansas shales were considered to be submarine, where they underwent ion exchange that lowered *REE* concentrations and reduced the *LREE*/*HREE* ratio because *HREE* are more resistant to exchange due to their higher charge/radius ratios (same charge of 3+ but smaller radius).

Shales and claystones of the Permian Irati formation in the Paraná Basin, Brazil, were investigated by Dos Anjos *et al.* (2010). The shales contained mainly saponite and mixed-layer talc-saponite, while the claystones consisted mainly of nontronite, with some lizardite and talc. The Mg- and Fe-rich clay minerals and basaltic accessory minerals pointed to basic or ultrabasic precursors, which was supported by *REE* values below those of average shales (Fig. 13). Only one sample had *REE* values above those of average shales, as well as a higher Al content, a low Mg content and a marked negative Ce anomaly, which led to this sample being interpreted as originating from the alteration of volcanic ash of intermediate composition in the sea. An andesitic composition for this sample was confirmed by geochemistry (plot of Zr/TiO_2 *vs* Nb/Y, not shown). Basaltic rocks have lower *REE* contents than felsic rocks because *REE* are incompatible; in other words, they are partitioned into magmas and late-crystallizing minerals, most significantly so for *LREE*, in every event of partial mantle melting (McLennan & Taylor, 2012).

Table 2. *R* values of binary correlations between Σ*REE* and elemental percentages in Arctic Ocean sediments at several distances from the mouth of the Lena River, Siberia. Negative values denote negative correlations (Ruban *et al.*, 2024).

	Al	K	Ti	Zr
Proximal	0.95	0.79	0.83	0.74
Medium	0.46	−0.10	0.79	0.70
Distal	−0.32	−0.40	0.40	0.84

Ruban *et al.* (2024) used *REE* to investigate the origins of the silty Arctic sediments of the Laptev Sea, between the Taymyr Peninsula and the New Siberian Islands, at increasing distance from the mouth of the Lena River. The *REE* patterns at proximal, medium and distal points had similar characteristics, with *LREE* > *HREE* and individual values between 0.6 and 1.5 *REE*/NASC, but with local variations of individual Ln concentrations. *REE* fractionation parameters ($Eu/Eu^* = Eu_N/0.5 \times (Sm_N + Gd_N)$; $Ce/Ce^* = Ce_N/0.5 \times (La_N + Pr_N)$; *LREE*/*HREE* expressed as $[La/Yb]_N$, $[Gd/Yb]_N$ and [La/Lu]; as well as $[Y/Ho]_N$, where N indicates NASC normalization) showed constant values in all proximal samples at all sample depths, whereas they varied widely with depth for medium and distal samples. These results indicated that proximal samples had a homogeneous source (i.e. the sediments from the Lena River). This inference was corroborated by the high positive correlation between Al, K and Ti with Σ*REE* (Table 2), all of which being usual elements in phyllosilicate-rich sediments.

The correlations of Al, K and Ti with Σ*REE* decreased rapidly and even became negative with distance from the Lena River, whereas the correlation with Zr remained high (Table 2). This was interpreted as demonstrating decreasing control of the Lena River sediments over the *REE* sediment composition (Ruban *et al.*, 2024). The fact that *REE* fractionation parameters varied with depth at medium and distal sediments was interpreted as being due to mixing of two sources that had variable inputs with time. The second source could potentially be the New Siberian Islands, located to the east and south-east of the medium and distal samples, respectively. The sediments closest to the New Siberian Islands had the coarsest particle size of all and the highest Σ*REE*, indicating the

https://doi.org/10.1180/clm.2026.10030 Published online by Cambridge University Press

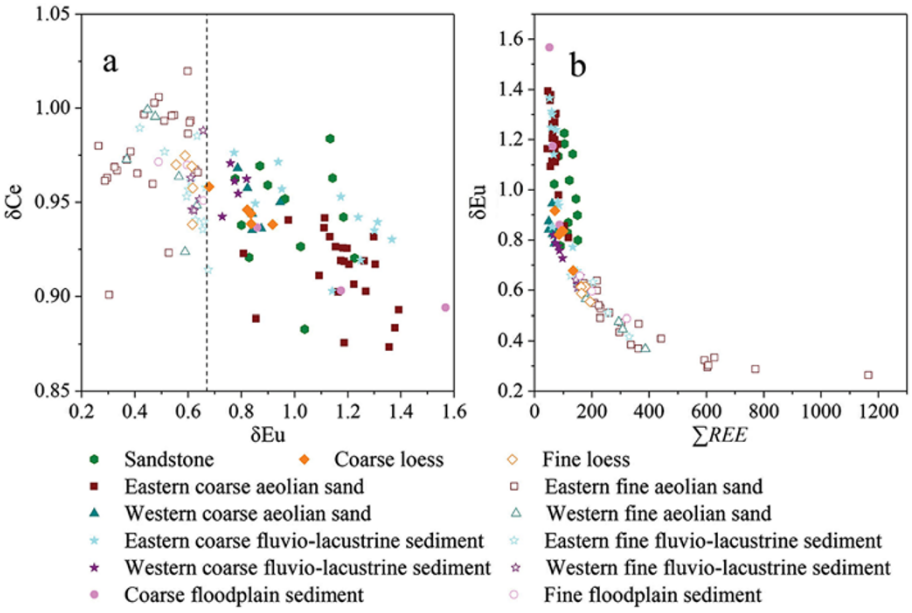


Figure 14. Plots of several *REE*-related variables allowing discrimination between coarse and fine sediments in the Mu Us Desert, China (Ding *et al.*, 2021): (a) δCe *vs* δEu and (b) δEu *vs* Σ*REE*. δEu and δCe are assumed to be identical to $Eu/Eu^* = Eu_N/(Sm_N \times Gd_N)^{0.5}$ and $Ce/Ce^* = Ce_N/(La_N \times Pr_N)^{0.5}$, but these were not defined by the authors.

presence of coarse-grained *REE*-rich minerals, such as monazite, zircon or titanite, as observed with SEM. All of these data and the principal component analysis (PCA) of geochemical, textural and mineralogical variables led Ruban *et al.* (2024) to conclude that the two sediment sources were the Lena River, mainly with phyllosilicate-borne *REE* and minor *REE*-rich minerals (detected monazite), and the New Siberian Islands, where *REE* were mainly in coarse-grained *REE*-rich minerals.

Sediment origin can be investigated using plots of *REE*-related variables that enhance the distinguishing characteristics of the *REE* patterns. In their investigation of Mu Us Desert sediments from north-central China, Ding *et al.* (2021), studied coarse and fine aeolian and fluvio-lacustrine sediments. The *REE* signatures of the fine and coarse fractions were different (presumably due to mineralogical control), and the *REE* values were higher for the fine fractions, due to them containing a greater proportion of clay minerals. Fines had a more pronounced negative Eu anomaly (lower δEu), and their Σ*REE* correlated with the depth of the Eu anomaly (i.e. higher Σ*REE* corresponded with lower δEu; Fig. 14b). By contrast, there was no correlation between Eu anomaly values and total *REE* concentrations for the coarse fraction (Fig. 14b). A plot of Ce and Eu anomalies discriminated coarse and fine fractions but did not show correlations between the two anomalies (Fig. 14a). Ding *et al.* (2021) built several pairwise variable plots (using δEu, $[Gd/Yb]_N$, La/Th and Zr/Hf) for the coarse and fine fractions of the several sediments and their possible sources. The origin of the coarse material could be discriminated because each sediment plotted closer to one of several sources. The fine fractions, however, appeared to be composed of a mixture of near and distant sources, such that they could not be linked to a particular source. This is an example of clay minerals losing their capacity to discriminate sources due to their ability to travel very long distances.

Investigation of sediments at the coastal Padre lagoon, Brazil, showed that *REE* concentration increased sharply above ∼40 cm depth, corresponding to 137–230 years before present, when Rio de Janeiro, 60 km away, industrialized and increased significantly in population (de Freitas *et al.*, 2023). This increment took place approximately where the sediment transitioned from a sandy mud to a muddy sand, in apparent contradiction to the fact that silt concentrates *REE* with respect to sand. Indeed, this latter fact was confirmed in this study because the analysis of separated size fractions showed higher *REE* concentrations in silt than in sand at all depths. The surface sediments had the highest sand content and yet they also had the highest *REE* concentrations. Such results suggested that, from 137 to 230 years ago, a new source of *REE* had been operating. Based on similar results worldwide, de Freitas *et al.* (2023) interpreted these results as indicating that the *REE* at depths >40 cm were provided by natural sediments, whereas the increase of *REE* at above 40 cm was due to particulate deposition of anthropogenic origin. They also suggested that sediment coarsening towards the surface was caused by the natural removal of fines through increased wave energy. Although not discussed by de Freitas *et al.* (2023), it can be added that anthropogenic input would take place mainly through wind transport and the deposition of fine particles. Some such particles of anthropogenic origin would release *REE* into the lagoon waters, and the *REE* then would be adsorbed on fine and coarse mineral particles. This would allow *REE* concentrations to increase towards the surface sediment even if the sand/silt ratio decreased, provided that the *REE* flux was sufficiently high.

Soil processes

Zang *et al.* (2024) investigated the *REE* signals of soil formation on clastic sediments and carbonates in Chongqing, south-west China, an area where both of these rock types crop out and have developed soils. Because the fine fractions concentrate *REE*, Zang *et al.* (2024) studied the clay fractions of carbonates, clastic rocks and their corresponding saprolites. *REE* abundance in the clay fractions of the saprolites was higher than in those of their precursors by 2.0–3.0 times for the carbonates and only 1.0–1.8 times for the clastic rocks. The main carriers of *REE* in carbonate rocks and corresponding saprolites were amorphous Fe oxides, followed by crystalline Fe oxides and then phyllosilicates. In the clastic materials, however, the order varied: amorphous Fe oxides > phyllosilicates > crystalline Fe oxides. Interestingly, the highest *REE* contents were detected in carbonate-derived saprolites.

https://doi.org/10.1180/clm.2026.10030 Published online by Cambridge University Press

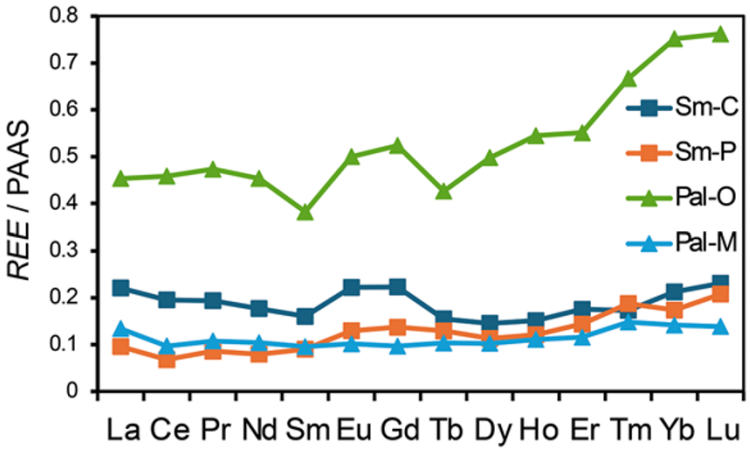


Figure 15. *REE* distributions in sediments that experienced early diagenesis within the Ganntour Basin, north-west Morocco. Sm-C and Sm-P are values from detrital smectite in a claystone and phosphorite, respectively. Pal-O and Pal-M are values from an authigenic palygorskite in a porcellanite (opal-CT-rich) and a dolomitic marl, respectively. Data from Chahi *et al.* (1999).

To trace the source of *REE*, Zang *et al.* (2024) calculated the La/Yb ratios (normalized to PAAS) for the bulks of both rocks and their corresponding soils on the one hand and for the corresponding fractions of amorphous Fe oxides, crystalline Fe oxides and phyllosilicates on the other. In plots of $(La/Yb)_N$ for soils *vs* their parent rocks of clastic materials, the data points approximately aligned along the 1:1 line, indicating that the soils inherited the *REE* distribution from their sediments of origin. However, for carbonates, the data points were above the 1:1 line and displayed no apparent pattern. This indicated that the *REE* had been fractionated. Possible fractionating processes were dissolution of carbonates, precipitation of new phases and concentration of pre-existing ones. This fractionation caused the increase in the *LREE*/*HREE* ratios. As phyllosilicates did not modify *REE* patterns (as shown in the clastic rocks), it was the Fe oxides that caused *LREE* concentration. Accordingly, this investigation established that incipient soil development on clastic sediments inherited, as expected, the precursor *REE* patterns, whereas the same process in carbonates modified the *REE* patterns by increasing the *LREE*/*HREE* ratio.

Not discussed by the authors, however, was that the *REE* patterns from one carbonate-derived soil showed a large Ce positive anomaly in amorphous Fe oxides, whereas the phyllosilicates presented an unremarkable negative Ce anomaly. Presumably, the Ce anomaly would be one more factor for establishing the process controlling *REE* distribution.

Diagenesis

Chahi *et al.* (1999) investigated the origins of smectite and palygorskite from the Ganntour Basin, north-west Morocco. During the Cretaceous–Tertiary, the basin was a shallow continental shelf that accumulated smectite and quartz from adjacent islands and large amounts of biogenic carbonate, phosphate and silica. Diagenesis of carbonate, phosphate and silica generated dolomite, apatite and opal-CT, respectively, while palygorskite and interstratified illite-smectite appeared in the dolomite- and opal-rich sediments. Representative samples were investigated: a claystone, a phosphorite, a dolomitic marl and a porcellanite (opal-CT), of which the first two contained smectite (labelled 'Sm-C' and 'Sm-P') and the latter two contained palygorskite (labelled 'Pal-M' and 'Pal-O'). After acid leaching to eliminate apatite contamination, the samples yielded approximately flat PAAS-normalized *REE* patterns (Fig. 15). Sample Sm-C, of assumed detrital origin, was considered compatible with altered acidic magmatic rocks due to its low *REE*/PAAS ratio. The presence of granites around the basin supported the notion that this particular smectite (Sm-C) was produced by meteoric weathering of the granitic rocks. Sample Sm-P produced *REE* patterns similar to those of Sm-C, albeit somewhat depleted in *LREE* (perhaps an effect of cation exchange in the shallow, organic-rich marine waters; Fig. 15), and Sm-P was also interpreted as detrital, with the same origin.

The two palygorskites had similar *REE* features to those of the smectites, although more pronounced and with greater concentration in Pal-O from the opal-rich environment (Fig. 15). Chahi *et al.* (1999) considered the higher *REE* concentration as consistent with the *REE* enrichment in biogenic siliceous marine environments, but we have not found support in the literature for such a claim, at least to the level of *REE* enrichment shown in Fig. 15. The patterns of Pal-O, however, suggest that Pal-O concentrated the *REE* content of Sm-C. Accordingly, the conclusion of Chahi *et al.* (1999) that Pal-O palygorskite was the result of the dissolution of detrital smectite and precipitation in the confined environment of the opal-rich environment is probable, but it requires that the mass of the precipitated palygorskite was substantially smaller than that of the dissolved smectite. Palygorskite precipitating after smectite dissolution was also the conclusion drawn for the marls (Pal-M), which was further supported by the fact that the $Al_2O_3/\Sigma REE$ ratios were similar for Sm-C and Pal-M. Such a similarity could be expected given that Al and *REE* are relatively immobile and that both would be retained in the neoformed palygorskite. In addition, the authors suggested that both palygorskites precipitated in non-oxidizing environments because they did not develop a negative Ce anomaly (Fig. 15).

Acid alteration

Areas in and around Riotinto (south-west Spain) have experienced acid alteration of varying intensity. Cuadros *et al.* (2023) investigated the products of a range of such alterations in silicate rock precursors with various characteristics. Mild acid alteration partially modified the mineralogical composition of the rock, resulting in pre-existing illite not affected by the alteration and newly formed kaolinite. Greater intensity of acid attack generated alunite, jarosite, beudantite and goethite (goethite was produced either directly or by later dissolution of jarosite). The various *REE* patterns of phyllosilicates (either original or newly formed, such as kaolinite) and the presence of sulfates and goethite enabled discrimination between mild and intense acid alteration (Fig. 16). The exception

https://doi.org/10.1180/clm.2026.10030 Published online by Cambridge University Press

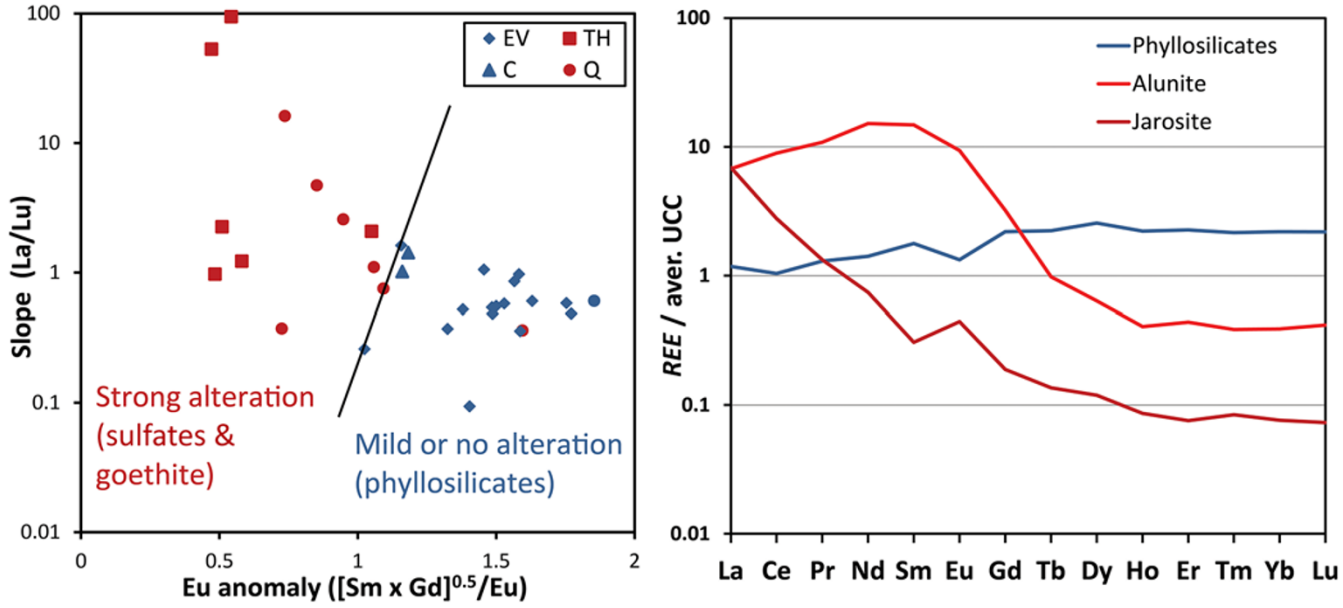


Figure 16. Modifications produced by acidic alteration of silicate rocks from various areas near Riotinto (south-west Spain). All measurements are from bulk rocks of complex mineralogy. The right panel shows examples of (1) mild alteration, with *REE* patterns dominated by the phyllosilicates, and (2) strong alteration, with *REE* patterns dominated by alunite and jarosite. The left panel displays a plot of two *REE* variables that allow discrimination of the effects of strong acidic alteration (red data points), producing sulfates and goethite. Only one sample that experienced strong acid alteration appeared in the mild alteration region (see text). The shapes of the data points and initials refer to their localities (C = Calañas; EV = El Villar; Q = Quebrantahuesos; TH = Tharsis). The Eu anomaly is here calculated as Eu*/Eu rather than the usual Eu/Eu*, as indicated on the *x*-axis. Data from Cuadros *et al.* (2023).

was a sample that contained beudantite (Fig. 16, red data point to the right of the dividing line), which showed a slight increase in *LREE* concentration *vs HREE*, as in the phyllosilicates, but also displayed a positive Eu anomaly, as in jarosite (Fig. 16). Cuadros *et al.* (2023) ascribed the shapes of the *REE* patterns of alunite and jarosite to the size of the crystallographic site that the *REE* occupy in these minerals, where *LREE* fit better than *HREE*. These measurements were carried out in bulk polymineralogical samples, meaning that the generation of patterns in bulk rock similar to those in Fig. 16 (right panel) can be used to infer acidic alteration.

REE ore clay mineral deposits

Description of the deposits

Since 1969, *REE* have been discovered to sufficiently concentrate in clay minerals within laterites to allow *REE* exploitation. Although the abundance of *REE* in these deposits is relatively low (0.05–0.20 wt.% rare earth oxides; Li & Zhou, 2020), their cost and ease of extraction make them economically viable (Moldoveanu & Papangelakis, 2016). They have become the main source of *HREE* globally, but not of *LREE*, which are found in greater amounts in other types of deposits (Wu *et al.*, 2023). These laterite deposits develop *via* thorough alteration of *REE*-rich rocks and concentration of *REE* in clay minerals by adsorption. For this reason, they are termed 'ion-adsorption *REE* deposits'. The original rocks are primarily *REE*-enriched granites (i.e. granites containing *REE*-rich minerals such as allanite, apatite, titanite, bastnäsite or fluorite). Less frequently, they are volcanic (rhyolite and dacite containing phosphates) and metamorphic rocks (meta-sandstone- and meta-tuff, phyllite, schist, slate and granulite containing *REE*-chlorite, *REE*-bearing Fe-Ti oxides, allanite and cerianite; Wu *et al.*, 2023). It is disputed whether adsorption deposits of commercial value can develop on carbonatites and basalts, and this is an area of current investigation (Wu *et al.*, 2023).

As lateritic environments are confined to tropical and subtropical areas and are young from a geologic perspective, such deposits are found in precisely the same areas, mainly in south China, followed by South-East Asia, Madagascar, Malawi and Brazil. Ancient laterites relocated by plate tectonics in non-tropical areas of the planet have also been reworked and lost or cemented, therefore ceasing to be *REE* deposits or usable *REE* deposits (Luo *et al.*, 2022). In addition to having low *REE* concentrations, lateritic deposits are also of small size (<10 kt of rare earth oxides; Li & Zhou, 2020). Given the characteristics of the precursor rock (granites) and high alteration, the most common clay minerals making up these deposits are kaolinite and halloysite, whereas smectite and illite are rare, in low concentrations and confined to the lower part of the alteration profile (Li & Zhou, 2020). The approximate structure of the deposits consists of humic topsoil (upper 0–2 m), a strongly weathered zone (5–10 m), semi-weathered saprolite (3–5 m) and slightly weathered protolith. Maximum *REE* concentrations are found in the strongly weathered and semi-weathered zones (Li & Zhou, 2020; Wu *et al.*, 2023).

As weathering progresses from top to bottom, some *REE* are bound by humic compounds or carbonate ions from the topsoil, whereas other Ln^{3+} are solvated, and these species percolate down the profile. This combined complexation and transport preferentially selects *HREE* over *LREE*, so that *LREE* are enriched in the upper part of the profile and *HREE* are enriched at the bottom. As *REE* species descend in the profile, the environmental pH increases, such that humic-complexed *REE* are detached and adsorb on the clay minerals (Wu *et al.*, 2023). The preferential adsorption of *HREE* by clay minerals, which are more abundant in the highly weathered middle zone, also increase *HREE* enrichment in the lower part of the profile. The mode of adsorption on the clay minerals is that described at the beginning of this review (i.e. *REE*

https://doi.org/10.1180/clm.2026.10030 Published online by Cambridge University Press

are coordinated by eight or nine oxygen atoms from phyllosilicate oxide ions and OH groups or H_2O molecules, whether in the interlayer space, at layer edges or at the external planar surface). Cerium is an exception due to its capacity to oxidize to Ce^{4+}, which results in the precipitation of cerianite (CeO_2) and a reduced extraction capacity by ion exchange (Estrade *et al.*, 2019; also see below).

The total proportion of clay minerals in these deposits ranges from 40% to 70% (Wu *et al.*, 2023). Their mineralogy consists of 10–60 wt.% kaolinite/halloysite, major to minor quartz, traces of smectite, minor to traces of vermiculite and illite/muscovite, metal oxides and oxy-hydroxides (Estrade *et al.*, 2019; Li & Zhou, 2020; Luo *et al.*, 2022), with variations in their proportions along the weathering profile (Wu *et al.*, 2023). Some 50–60% of *REE* are retained in kaolinite/halloysite, although this value sometimes reaches up to 90%; up to 30% of *REE* are retained in residual *REE*-rich minerals (e.g. phosphates, cerianite, allanite), ~3% are retained in metal oxy-hydroxides, <1% are retained in OM and small proportions are retained in carbonates (Li & Zhou, 2020; Wu *et al.*, 2023).

REE *extraction from ion-adsorption deposits*

Although beneficiation is not required for *REE* extraction in ion-adsorption deposits, the variety of minerals, mineral sites and bonds that retain *REE* means that extraction requires several sequential processes. However, the focus in this review is on the phyllosilicate-retained *REE*, which is also the large majority of *REE* in this type of deposit. *REE* are mobilized from phyllosilicates by cation exchange. The process follows the thermodynamic rules of cation exchange with which many clay scientists are familiar. Both the cation and anion of the salt added to remove *REE* modify the efficiency of the removal. The salt most commonly used is ammonium sulfate (Wu *et al.*, 2023). The double charge of the anion provides two cations per mole, which increases exchange. However, economic factors are also important in the choice of the exchanging salt. Because ammonium sulfate needs to be added in large excess to achieve efficient exchange, this method causes ammonium contamination. Ammonium reduction is achieved by mixing exchanging cations, such as in combinations of $(NH_4)_2SO_4$, $MgSO_4$, $CaCl_2$ and $FeSO_4$ (Wu *et al.*, 2023). Exchange efficiency in excess of 80% is typically achieved.

For optimized exchange efficiency (>80%), the molar ratio of $(NH_4)_2SO_4$ to adsorbed *REE* is 18 (Moldoveanu & Papangelakis, 2013), and greater such ratios do not result in greater efficiency (Wu *et al.*, 2023). Solid-to-liquid ratios also follow the usual thermodynamic rules. Even if the salt/*REE* ratio is appropriate, a high solid-to-liquid ratio decreases the efficient migration of cations to and from the mineral surface, causing apparent saturation and resulting in inefficient exchange. However, too low solid-to-liquid ratios disperse the exchange cations in the liquid far from the mineral surfaces, thereby also reducing efficiency. An example has been described in which the transitions of solid-to-liquid ratios from 10/3 → 10/7 → 10/11 translated into efficiency modifications of 66% → 95% → 97% (Wu *et al.*, 2023). The higher efficiency at the 10/11 ratio may not counteract the disadvantage of the higher *REE* dilution in the resulting solution. The pH range for the most efficient conditions is 3–5, where *REE* are mainly as $Ln(OH_2)_{8-9}$ complexes or mixed aquo-phyllosilicate surface complexes while, simultaneously, phyllosilicate dissolution (pH < 3) and hydroxy complexes (pH > 5) are avoided (Fig. 1). In addition, this pH range promotes carbonate dissolution and mobilization of the corresponding *REE* (Estrade *et al.*, 2019). The time required to reach maximum exchange in batch experiments is 5 min (Moldoveanu & Papangelakis, 2013). Moderate improvements (10–20%) in *REE* desorption have been obtained in experiments using organic chelates to bind the desorbed *REE* (Moldoveanu & Papangelakis, 2021).

After exchange, the *REE*-bearing solution also contains large amounts of cations from the clay minerals and associated oxides and oxy-hydroxides, mainly Al and Fe. They are separated by adjusting the pH so that Al and Fe can precipitate as hydroxides while the *REE* remain in solution. Such pH values fall within a narrow range of 4.8–5.2, which has been achieved using ammonium bicarbonate and ammonia. More recently, selective organic ligands have been developed that bind Al and Fe strongly and avoid their precipitation (Luo *et al.*, 2022). The *REE* are extracted from the liquid using several processes. They can be precipitated using oxalic acid or ammonium bicarbonate, which generate the corresponding oxalate ($Ln_2(C_2O_4)$) and carbonate compounds ($Ln_2(CO_3)_3$). They can also be extracted using a solvent extractant or a 'liquid membrane' (i.e. an emulsion with a carrier), where *REE* can penetrate emulsion droplets and be retained there, and then the emulsion is separated from the liquid (Luo *et al.*, 2022).

Conclusions

Phyllosilicates of all particle sizes, from the macrocrystalline to the clay minerals group, have a complex crystal chemistry that allows for multiple combinations of cations, site occupancies and vacancies. Such possibilities mean that they are responsive to environmental modifications and can react in almost any direction of the multi-dimensional space defined by the multiple variables of chemical composition, temperature, pH, Eh and gas partial pressure, although their reaction kinetics are generally slow. Such a combination of reactivity, crystal chemical flexibility and inertia to transformation makes them successful tracers of past environments, whether climate- or geology-driven (e.g. Fagel, 2024). Importantly, these properties enable the generation of 'halfway' mineral phases of two or three components: the interstratified clay minerals, which contribute process and mechanistic information (Cuadros, 2021). And yet, clay mineral reaction kinetics are increased drastically in certain environments, particularly where they are controlled by Fe reduction and/or in saline waters (Cuadros *et al.*, 2017). Finally, clay minerals can react along multiple pathways, from bulk dissolution and reprecipitation to solid-state modification (e.g. Baldermann, 2013; Cuadros, 2021).

Such a number and complexity of possibilities does not, in principle, suggest a simple interaction with *REE* or that phyllosilicates will be appropriate *REE* hosts to be used as tracers of precursor rocks or geological processes. Nonetheless, three facts cause *REE*–phyllosilicate systems to be good tracers of the geological past: (1) *REE* bind to all phyllosilicates in a single way and across most of the pH range (Fig. 1); (2) they bind strongly; and (3) they bind at multiple sites. *REE* bind to phyllosilicates through adsorption only, forming complexes with combinations of water, oxide and hydroxide groups, at the interlayer of swelling clay minerals and on the outer surfaces of all phyllosilicates. This similarity of binding across clay minerals and environmental conditions simplifies phyllosilicate–*REE* interactions drastically. Furthermore, the multiple sites available for *REE* sorption and the high binding strength cause *REE* to successfully compete for adsorption sites on phyllosilicates, and for the latter to be very effective at retaining *REE*. *REE* have combined large radii and high charge, excluding them from substituting cations beyond trace concentrations

https://doi.org/10.1180/clm.2026.10030 Published online by Cambridge University Press

in most major rock-forming minerals and secondary sedimentary minerals (McLennan, 1989). *REE* sorption on mineral surfaces does not occur to a large extent because most minerals have electrically neutral crystal lattices and/or have small surface areas, with the exception of clay minerals and metal oxides and oxyhydroxides.

As a consequence, phyllosilicates retain a large proportion of the *REE* present in precursor rocks and retain them strongly, enabling the tracing of the origins of sediments, even after long-distance transport, long periods of time and across a wide range of modifications to environmental conditions. Replacement of silicates of all types by phyllosilicates, no matter the reaction mechanism, typically preserves the *REE* signature. Natural aqueous solutions carry low concentrations of *REE* and have limited ability to modify the *REE* signatures of clay minerals unless under extreme conditions of pH, concentrations of effective *REE*-complexing anions and concentrations of OM and metal oxide nanoparticles, especially where these solutions operate for a long period of time. In these situations, phyllosilicates can be good tracers of the corresponding geological processes. The examples and discussions provided above, however, show that multiple factors can modify *REE* concentrations in phyllosilicates, and that identifying the geological processes responsible for such modifications may not be straightforward or even possible in complex processes or when several processes are juxtaposed. Geological, mineralogical, physical and chemical factors can nevertheless help constrain the operating processes.

The same reasons allow clay minerals, particularly kaolinite and halloysite, to become viable *REE* deposits. Clay minerals can capture the *REE* freed by the dissolution of other minerals, concentrate them and retain them. At the same time, they can easily and inexpensively be mobilized and separated in mining operations through cation-exchange and complexation reactions, with the ease of such mining processes balancing the low deposit contents and concentrations in the rock. These 'ionic' deposits have quickly become the primary source of *HREE* globally.

It is not yet clear whether all clay minerals have the same *REE* retention and segregation capacities or whether there are substantial differences intrinsic to their mineralogy or dependent on variables such as crystal order, surface area and negative tetrahedral and octahedral charge, or rather that the variability of retention or segregation between the different minerals is generated by environmental conditions (e.g. pH, fluid composition or ion concentration). Generally, studies from natural settings showed no or limited such differences (e.g. Cullers *et al.*, 1975; Elderfield *et al.*, 1990), whereas some laboratory investigations using individual clay minerals indicated significant such differences (e.g. Alshameri *et al.*, 2019). This contrast may be due to the homogenizing effect of complex clay mineral mixtures. Calculation of the binding energy between specific *REE* and the several sites identified in the several phyllosilicates is now possible using computational tools, and this represents a desirable first approach to identifying possible differences in well-controlled conditions. The issue is interesting in terms of fundamental knowledge regarding phyllosilicate–*REE* interactions, but it may be too convoluted in its manifestation in natural environments (e.g. involving multiple mineral and environmental variables) to be definitively solved or to be of use for unravelling processes and identifying precursors.

Competing interests. The authors declare none.

References

Aagaard P. (1974) Rare earth elements adsorption on clay minerals. *Bulletin du Groupe Français des Argiles*, **6**, 193–199.

Abanda P.A. & Hannigan R.E. (2006) Effect of diagenesis on trace element partitioning in shales. *Chemical Geology*, **230**, 42–59.

Abbott A.N., Löhr S. & Trethewy M. (2019) Are clay minerals the primary control on the oceanic rare earth element budget? *Frontiers in Marine Science*, **6**, 504.

Ahmadnejad F., Zamanian H., Taghipour B., Zarasvandi A., Buccione R. & Ellahi S.S. (2017) Mineralogical and geochemical evolution of the Bidgol bauxite deposit, Zagros Mountain Belt, Iran: implications for ore genesis, rare earth elements fractionation and parental affinity. *Ore Geology Reviews*, **86**, 755–783.

Aide M.T. & Aide C. (2012) Rare earth elements: their importance in understanding soil genesis. *International Scholarly Research Notices*, **2012**, 783876.

Alshameri A., He H., Xin C., Zhu J., Xinghu W., Zhu R. & Wang H. (2019) Understanding the role of natural clay minerals as effective adsorbents and alternative source of rare earth elements: adsorption operative parameters. *Hydrometallurgy*, **185**, 149–161.

Álvarez-Vázquez M.Á., De Uña-Álvarez E. & Prego R. (2022) Patterns and abundance of rare earth elements in sediments of a bedrock river (Miño River, NW Iberian Peninsula). *Geosciences*, **12**, 105.

Andrade G.R.P., Cuadros J., Barbosa J.M.P. & Vidal-Torrado P. (2022) Clay minerals control rare earth elements (*REE*) fractionation in Brazilian mangrove soils. *Catena*, **209**, 105855.

Arienzo M., Ferrara L., Trifuoggi M. & Toscanesi M. (2022) Advances in the fate of rare earth elements, *REE*, in transitional environments: coasts and estuaries. *Water*, **14**, 401.

Ayora C., Macías F., Torres E. & Nieto J.M. (2015) Rare earth elements in acid mine drainage. Presented at: *XXXV Reunión de la Sociedad Española de Mineralogía*. Huelva, Spain, 30 June–3 July. Contribution S3, p. 22.

Babu S.S., Venkata Ramana R., Purnachandra Rao V., Ram Mohan M., Sawant S., Satyasree N. & Keshav Krishna A. (2021) Rare earth elements of sediments in rivers and estuaries of the east coast of India. *Current Science*, **120**, 519–537.

Balashov Y.A. & Girin Y.P. (1969) On the reserve of mobile rare earth elements in sedimentary rocks. *Geochemistry International*, **6**, 649–659.

Baldermann A., Warr L.N., Grathoff G.H. & Dietzel M. (2013) The rate and mechanism of deep-sea glauconite formation at the Ivory Coast–Ghana Marginal Ridge. *Clays and Clay Minerals*, **61**, 258–276.

Bart S.C. (2023) What is the 'lanthanide contraction'? *Inorganic Chemistry*, **62**, 3713–3714.

Bayon G., Toucanne S., Skonieczny C, André L., Bermell S., Cheron S. *et al.* (2015) Rare earth elements and neodymium isotopes in world river sediments revisited. *Geochimica et Cosmochimica Acta*, **170**, 17–38.

Bayon G., Giresse P., Chen H., Rouget M.-L., Gueguen B., Moizinho G.R. *et al.* (2023) The behavior of rare earth elements during green clay authigenesis on the Congo continental shelf. *Minerals*, **13**, 1081.

Benson E.K. & Watts K.E. (2024) Apatite and monazite geochemistry record magmatic and metasomatic processes in rare earth element mineralization at Mountain Pass, California. *Economic Geology*, **119**, 1611–1642.

Berti D., Slowey N.C., Yancey T.E. & Deng Y. (2022) Rare earth nanominerals in bentonite deposits of the Eocene Texas coastal plains. *Applied Clay Science*, **216**, 106373.

Bobos I. & Gomes C. (2021) Mineralogy and geochemistry (HFSE and *REE*) of the present-day acid-sulfate types alteration from the active hydrothermal system of Furnas Volcano, São Miguel Island, the Azores Archipelago. *Minerals*, **11**, 335.

Borst A.M., Smith M.P., Finch A.A., Estrade G., Villanova-de-Benavent C., Nason P. *et al.* (2020) Adsorption of rare earth elements in regolith-hosted clay deposits. *Nature Communications*, **11**, 4386.

Bradbury M.H. & Baeyens B. (2002) Sorption of Eu on Na- and Ca-montmorillonites: experimental investigations and modelling with cation exchange and surface complexation. *Geochimica et Cosmochimica Acta*, **66**, 2325–2334.

https://doi.org/10.1180/clm.2026.10030 Published online by Cambridge University Press

Brady P.V. & Walther J.V. (1989) Controls on silicate dissolution rates in neutral and basic pH solutions at 25°C. *Geochimica et Cosmochimica Acta*, **53**, 2823–2830.

Brantley S.L. (2008) Kinetics of mineral dissolution. Pp. 151–210 in: S.L. Brantley, J.D. Kubicki & A.F. White (eds), *Kinetics of Water–Rock Interaction*. Springer, New York, NY, USA.

Brookins D.G., 1989. Aqueous geochemistry of rare earth elements. Pp. 201–225 in: B.R. Lipin & G.A. McKay (eds), *Geochemistry and Mineralogy of Rare Earth Elements*. Reviews in Mineralogy, vol. 21. Mineralogical Society of America, Washington, DC, USA.

Bruque S., Mozas T. & Rodríguez A. (1980) Factors influencing retention of lanthanide ions by montmorillonite. *Clay Minerals*, **15**, 413–420.

Cantrell K.J. & Byrne R.H. (1987) Rare earth element complexation by carbonate and oxalate ions. *Geochimica et Cosmochimica Acta*, **51**, 597–606.

Cascante M.D., Wu C.-Y. & Hseu Z.-Y. (2025) Fractionation of rare earth elements in tropical soils from marine mudstone along a toposequence. *Heliyon*, **11**, e42097.

Chahi A., Clauer N., Toulkeridis T. & Bouabdelli M. (1999) Rare-earth elements as tracers of the genetic relationship between smectite and palygorskite in marine phosphorites. *Clay Minerals*, **34**, 419–427.

Chakhmouradian A.R. & Wall F. (2012) Rare earth elements: minerals, mines, magnets (and more). *Elements*, **8**, 333–340.

Chamley H. (1989). Aeolian input. Pp. 133–161 in: *Clay Sedimentology*. Springer, Berlin, Germany.

Christidis G.E. (1998). Comparative study of the mobility of major and trace elements during alteration of an andesite and a rhyolite to bentonite, in the islands of Milos and Kimolos, Aegean, Greece. *Clays and Clay Minerals*, **46**, 379–399.

Cidu R., Antisari L.V., Biddau R., Buscaroli A., Carbone S., Da Pelo S. *et al.* (2013) Dynamics of rare earth elements in water–soil systems: the case study of the Pineta San Vitale (Ravenna, Italy). *Geoderma*, **193–194**, 52–67.

Condie K.C. (1991) Another look at rare earth elements in shales. *Geochimica et Cosmochimica Acta*, **55**, 2527–2531.

Coppin F., Berger G., Bauer A., Castet S. & Loubet M. (2002) Sorption of lanthanides on smectite and kaolinite. *Chemical Geology*, **182**, 57–68.

Cormack D. & Bowen V.T. (1967) *Lanthanide Interaction with Particles in Sea Water. I. Standard Clay Minerals*. Report NYO-2174-53. Woods Hole Oceanographic Institute, Woods Hole, MA, USA.

Cuadros J. (2006) Modeling of smectite illitization in burial diagenesis environments. *Geochimica et Cosmochimica Acta*, **70**, 4181–4195.

Cuadros J. (2021) Clay crystal-chemical adaptability and transformation mechanisms. *Clay Minerals*, **47**, 147–164.

Cuadros J., Andrade G., Ferreira T.O., Partiti C.S.M., Cohen R. & Vidal-Torrado P. (2017) The mangrove reactor: fast clay transformation and potassium sink. *Applied Clay Science*, **140**, 50–58.

Cuadros J., Mavris C. & Nieto J.M. (2023) Rare earth element signature modifications induced by differential acid alteration of rocks in the Iberian Pyrite Belt. *Chemical Geology*, **619**, 121323.

Cullers R.L. (1995) The controls on the major- and trace-element evolution of shales, siltstones and sandstones of Ordovician to Tertiary age in the Wet Mountains region, Colorado, U.S.A. *Chemical Geology*, **123**, 107–131.

Cullers R.L., Chaudhuri S., Arnold B., Lee M. & Wolf C.W. (1975) Rare earth distributions in clay minerals and in the clay-sized fraction of the Lower Permian Havensville and Eskridge shales of Kansas and Oklahoma. *Geochimica et Cosmochimica Acta*, **39**, 1691–1703.

da Silva Y.J.A.B., Araújo do Nascimento C.W.A., Biondi C.M., van Straaten P., de Souza Júnior V.S., da Silva Y.J.A.B. *et al.* (2017) Influence of metaluminous granite mineralogy on the rare earth element geochemistry of rocks and soils along a climosequence in Brazil. *Geoderma*, **306**, 28–39.

da Silva Y.J.A.B., Araújo do Nascimento C.W., Biondi C.M., van Straaten P. & da Silva Y.J.A.B. (2018) Rare earth element geochemistry during weathering of S-type granites from dry to humid climates of Brazil. *Journal of Plant Nutrition and Soil Science*, **181**, 938–953.

de Freitas A.S., Pompermayer L.L.O., Santos A.D.O., do Nascimento M.T.L., Saint'Pierre T.D., Hauser-Davis R.A. *et al.* (2023) Rare earth elements as sediment contamination tracers in a coastal lagoon in the state of Rio de Janeiro, Brazil. *Journal of Trace Elements and Minerals*, **4**, 100068.

Ding J., Wu Y., Tan L., Fu T., Du S., Wen Y. & Li D. (2021) Trace and rare earth element evidence for the provenances of aeolian sands in the Mu Us Desert, NW China. *Aeolian Research*, **50**, 100683.

Dos Anjos C.W.D., Meunier A., Guimarães E.M. & El Albani A. (2010) Saponite-rich black shales and nontronite beds of the Permian Irati Formation: sediment sources and thermal metamorphism (Paraná Basin, Brazil). *Clays and Clay Minerals*, **58**, 606–626.

Dubinin A.V. & Sval'nov V.N. (2003) Geochemistry of the manganese ore process in the ocean: evidence from rare earth elements. *Lithology and Mineral Resources*, **38**, 91–100.

Duddy L.R. (1980) Redistribution and fractionation of rare-earth and other elements in a weathering profile. *Chemical Geology*, **30**, 363–381.

Dutrizac J.E. (2017) The behaviour of the rare earth elements during gypsum ($CaSO_4{\cdot}2H_2O$) precipitation. *Hydrometallurgy*, **174**, 38–46.

Edzwald J.K. & O'Melia C.R. (1975) Clay distributions in recent estuarine sediments. *Clays and Clay Minerals*, **23**, 39–44.

Elderfield H., Upstill-Goddard R. & Sholkovitz E.R. (1990) The rare earth elements in rivers, estuaries, and coastal seas and their significance to the composition of ocean waters. *Geochimica et Cosmochimica Acta*, **54**, 971–991.

Estrade G., Marquis E., Smith M., Goodenough K. & Nason P. (2019) *REE* concentration processes in ion adsorption deposits: evidence from the Ambohimirahavavy alkaline complex in Madagascar. *Ore Geology Reviews*, **112**, 103027.

Fagel N. (2024) Climatic significance of clay minerals in Cenozoic marine and lacustrine sediments. *Clay Minerals*, **59**, 228–257.

Febina A.M. & Priya K.L. (2024) Analysing the role of Fe(II) on flocculation of sand–clay mixtures under estuarine mixing. *Environmental Research*, **251**, 118590.

Feng J.-L., Hu Z.-G., Ju J.-T. & Zhu L.-P. (2011) Variations in trace element (including rare earth element) concentrations with grain sizes in loess and their implications for tracing the provenance of aeolian deposits. *Quaternary International*, **236**, 116–126.

Feng X., Onel O., Council-Troche M., Noble A., Yoon R.H. & Morris J.R. (2021) A study of rare earth ion-adsorption clays: the speciation of rare earth elements on kaolinite at basic pH. *Applied Clay Science*, **201**, 105920.

Fernández-Caliani J.C. (2018) Rare-earth element and stable isotope signatures of kaolin from a Pliocene lateritic weathering profile at mid-latitude region (Andalusia, Spain): implications for paleoweathering and paleoclimatic reconstructions. *Catena*, **167**, 160–170.

Ferrat M., Weiss D.J., Strekopytov S., Dong S., Chen H., Najorka J. *et al.* (2011) Improved provenance tracing of Asian dust sources using rare earth elements and selected trace elements for palaeomonsoon studies on the eastern Tibetan Plateau. *Geochimica et Cosmochimica Acta*, **75**, 6374–6399.

Fleet A.J., Buckley H.A. & Johnson L.R. (1980) The rare earth element geochemistry of glauconites and celadonites. *Journal of the Geological Society of London*, **137**, 683–688.

Fontaine F., Christidis G.E., Yans J., Hollanders S., Hoffman A. & Fagel N. (2020). Characterization and origin of two Fe-rich bentonites from Westerwald (Germany). *Applied Clay Science*, **187**, 105444.

Freslon N., Bayon G., Toucanne S., Bermell S., Bollinger C., Chéron S. *et al.* (2014) Rare earth elements and neodymium isotopes in sedimentary organic matter. *Geochimica et Cosmochimica Acta*, **140**, 177–198.

Fulignati P., Gioncada A. & Sbrana A. (1999) Rare-earth element (*REE*) behaviour in the alteration facies of the active magmatic–hydrothermal system of Vulcano (Aeolian Islands, Italy). *Journal of Volcanology and Geothermal Research*, **88**, 325–342.

Galán E., Fernández-Caliani J.C., Miras A., Aparicio P., Márquez M.G. (2007) Residence and fractionation of rare earth elements during kaolinization of alkaline peraluminous granites in NW Spain. *Clay Minerals*, **42**, 341–352.

Gammons C.H., Wood S.A., Pedrozo F., Varekamp J.C., Nelson B.J., Shope C.L. & Baffico G. (2005) Hydrogeochemistry and rare earth element behavior in a volcanically acidified watershed in Patagonia, Argentina. *Chemical Geology*, **222**, 249–267.

Gimeno-Serrano M.J., Auqué-Sanz L.F. & Nordstrom D.K. (2000) *REE* speciation in low temperature acidic waters and the competitive effects of aluminum. *Chemical Geology*, **165**, 167–180.

https://doi.org/10.1180/clm.2026.10030 Published online by Cambridge University Press

Goldstein S.J. & Jacobsen S.B. (1988) Rare earth elements in river waters. *Earth and Planetary Science Letters*, **89**, 35–47.

Goodenough K., Wall F. & Merriman D. (2018). The rare earth elements: demand, global resources, and challenges for resourcing future generations. *Natural Resources Research*, **27**, 201–216.

Greaves M.J., Elderfield H. & Sholkovitz E.R. (1999) Aeolian sources of rare earth elements to the western Pacific Ocean. *Marine Chemistry*, **68**, 31–38.

Gruau G., Dia A., Olivié-Lauquet G., Davranche M. & Pinay G. (2004) Controls on the distribution of rare earth elements in shallow groundwaters. *Water Research*, **38**, 3576–3586.

Gurvich E.G. (2006) *Metalliferous Sediments of the World Ocean*. Springer, Berlin, Germany, 416 pp.

Heines M., Khot V. & Strous M. (2023) The vigor, futility, and applications of microbial element cycles in alkaline soda lakes. *Elements*, **19**, 30–36.

Howard J.J. & Roy D.M. (1985) Development of layer charge and kinetics of experimental smectite alteration. *Clays and Clay Minerals*, **33**, 81–88.

Huertas F.J., Chou L. & Wollast R. (1999) Mechanism of kaolinite dissolution at room temperature and pressure. Part II: kinetic study. *Geochimica et Cosmochimica Acta*, **63**, 3261–3275.

Huggett J., Adetunji J., Longstaffe F. & Wray D. (2017) Mineralogical and geochemical characterisation of warm-water, shallow-marine glaucony from the Tertiary of the London Basin. *Clay Minerals*, **52**, 25–50.

Iannicelli-Zubiani E.M., Cristiani C., Dotelli G., Gallo Stampino P., Pelosato R., Mesto E. *et al.* (2015) Use of natural clays as sorbent materials for rare earth ions: materials characterization and set up of the operative parameters. *Waste Management*, **46**, 546–556.

Johannesson K.H. & Xiaoping Z. (1997) Geochemistry of the rare earth elements in natural terrestrial waters: a review of what is currently known. *Chinese Journal of Geochemistry*, **16**, 20–42.

Johannesson K.H., Lyons W.B., Stetzenbach K.J. & Byrne R.H. (1995) The solubility control of rare earth elements in natural terrestrial waters and the significance of PO_4^{3-} and CO_3^{2-} in limiting dissolved rare earth concentrations: a review of recent information. *Aquatic Geochemistry*, **1**, 157–173.

Johannesson K.H., Stetzenbach K.J., Hodge V.F. & Lyons W.B. (1996) Rare earth element complexation behavior in circumneutral pH groundwaters: assessing the role of carbonate and phosphate ions. *Earth and Planetary Science Letters*, **139**, 305–319.

Karakaya M.Ç., Karakaya N. & Küpeli Ş. (2011) Mineralogical and geochemical properties of the Na- and Ca-bentonites of Ordu (NE Turkey). *Clays and Clay Minerals*, **59**, 75–94.

Kawamura K. & Kaplan I.R. (1987) Dicarboxylic acids generated by thermal alteration of kerogen and humic acids. *Geochimica et Cosmochimica Acta*, **51**, 3201–3207.

Kaya M., Yildirim B.A., Kumral M. & Sasmaz A. (2023) Trace and rare earth element (*REE*) geochemistry of recently formed stromatolites at Lake Salda, SW Turkey. *Water*, **15**, 733.

Kiipli T., Rutt Hints R., Kallaste T., Verš E. & Voolma M. (2017) Immobile and mobile elements during the transition of volcanic ash to bentonite – an example from the early Palaeozoic sedimentary section of the Baltic Basin. *Sedimentary Geology*, **347**, 148–159.

Kikawada Y., Fukaia M. & Oia T. (2013) Specific *REE* patterns observed in sulfurous hot springs from a hydrothermal alteration area in Manza, Japan. *Procedia Earth and Planetary Science*, **7**, 428–431.

Kreitsmann T., Kraemer D., Mahecha A., Regenspurg S., Wilke F.D.H. & Bau M. (2023) Rare earth elements and yttrium in alkaline lakes and hot springs from Tanzania. Presented at: *Goldschmidt Conference*, Lyon, France, 9–14 July. Paper 17851, abstract 10337.

Krull-Davatzes A.E., Lowe D.R. & Byerly G.R. (2012) Mineralogy and diagenesis of 3.24Ga meteorite impact spherules. *Precambrian Research*, **196–197**, 128–148.

Lackschewitz K.S., Singer A., Botz R., Garbe-Schönberg D., Stoffers P. & Horz K. (2000) Formation and transformation of clay minerals in the hydrothermal deposits of Middle Valley, Juan de Fuca Ridge, ODP Leg 169. *Economic Geology*, **95**, 361–389.

Laurila T.E., Hannington M.D., Petersen S. & Garbe-Schönberg D. (2014) Early depositional history of metalliferous sediments in the Atlantis II Deep of the Red Sea: evidence from rare earth element geochemistry. *Geochimica et Cosmochimica Acta*, **126**, 146–168.

Laveuf C. & Cornu S. (2009) A review on the potentiality of rare earth elements to trace pedogenetic processes. *Geoderma*, **154**, 1–12.

Lawrence C.R. & Neff J.C. (2009) The contemporary physical and chemical flux of aeolian dust: a synthesis of direct measurements of dust deposition. *Chemical Geology*, **267**, 46–63.

Li B., Kong Q., Wang G., Liu F., Guo L., Liu C. *et al.* (2022) Controls on the behaviors of rare earth elements in acidic and alkaline thermal springs. *Applied Geochemistry*, **143**, 105379.

Li C.-S., Shi X.-F., Kao S.-J., Liu Y.-G., Lyu H.-H. Zou J.-J. *et al.* (2013) Rare earth elements in fine-grained sediments of major rivers from the high-standing island of Taiwan. *Journal of Asian Earth Sciences*, **69**, 39–47.

Li M.Y.H. & Zhou M.F. (2020) The role of clay minerals in formation of the regolith-hosted heavy rare earth element deposits. *American Mineralogist*, **105**, 92–108.

Liu H., Guo H., Pourret O., Wang Z., Sun Z., Zhang W. & Liu M. (2021) Distribution of rare earth elements in sediments of the North China Plain: a probe of sedimentation process. *Applied Geochemistry*, **134**, 105089.

Liu M. & Han G. (2021) Distribution and fractionation of rare earth elements in suspended particulate matter in a coastal river, southeast China. *PeerJ*, **29**, e12414.

Liu X. & Byrne R.H. (1998) Comprehensive investigation of yttrium and rare earth element complexation by carbonate ions using ICP-mass spectrometry. *Journal of Solution Chemistry*, **27**, 803–815.

Liu X., Tournassat C., Grangeon S., Kalinichev S., Takahashi Y. & Fernandes M.M. (2022) Molecular-level understanding of metal ion retention in clay-rich materials. *Nature Reviews Earth and Environment*, **3**, 461–476.

Lottermoser B.G. (1992) Rare earth elements and hydrothermal ore formation processes. *Ore Geology Reviews*, **7**, 25–41.

Luo X., Zhang Y., Zhou H., He K., Luo C., Liu Z. & Tang X. (2022) Review on the development and utilization of ionic rare earth ore. *Minerals*, **12**, 554.

Mariano A.N. (1989) Economic geology of rare earth minerals. Pp. 309–338 in: B.R. Lipin & G.A. McKay (eds), *Geochemistry and Mineralogy of Rare Earth Elements*. Reviews in Mineralogy, vol. 21. Mineralogical Society of America, Washington, DC, USA.

Martínez J.A., Jiménez de Cisneros C. & Caballero E. (2007) Natural acid sulphate alteration in bentonites (Cabo de Gata, Almería, SE Spain). *Clay Minerals*, **42**, 89–107.

Martínez-Ruiz F., Ortega-Huertas M. & Rivas P. (2006) Rare earth element composition as evidence of the precursor material of Cretaceous–Tertiary boundary sediments at distal sections. *Chemical Geology*, **232**, 1–11.

Maslov A.V. (2021) Volcanic tuffs, red- and usual-colored clayey rocks in Upper Riphean–Vendian deposits in the Middle and Southern Urals: comparison of lithochemical characteristics. *Lithology and Mineral Resources*, **56**, 132–151.

Mavris C., Cuadros J., Nieto J.M., Bishop J.L. & Michalski J.R. (2018) Diverse mineral assemblages of acidic alteration in the Rio Tinto area (southwest Spain): implications for Mars. *American Mineralogist*, **103**, 1877–1890.

McLennan S.M. (1989) Rare earth elements in sedimentary rocks: influence of provenance and sedimentary processes. Pp. 169–200 in: B.R. Lipin & G.A. McKay (eds), *Geochemistry and Mineralogy of Rare Earth Elements*. Reviews in Mineralogy, vol. 21. Mineralogical Society of America, Washington, DC, USA.

McLennan S.M. (2001) Relationships between the trace element composition of sedimentary rocks and upper continental crust. Geochemistry, Geophysics, Geosystems, **2**, 2000GC000109.

McLennan S.M. & Taylor S.R. (2012) Geology, geochemistry and natural abundances. *Encyclopedia of Inorganic and Bioinorganic Chemistry*. Wiley Online Library. Retrieved from https://doi.org/10.1002/9781119951438.eibc2004.

Michard A. (1989) Rare earth element systematics in hydrothermal fluids. *Geochimica et Cosmochimica Acta*, **53**, 745–750.

Michard A. & Albarède F. (1986) The *REE* content of some hydrothermal fluids. *Chemical Geology*, **55**, 51–60.

Miller S.E., Heath G.R. & Gonzalez R.D. (1982) Effects of temperature on the sorption of lanthanides by montmorillonite. *Clays and Clay Minerals*, **30**, 111–122.

Millero F.J. (1992) Stability constants for the formation of rare earth inorganic complexes as a function of ionic strength. *Geochimica et Cosmochimica Acta*, **56**, 3123–3132.

https://doi.org/10.1180/clm.2026.10030 Published online by Cambridge University Press

Mitra S., Gupta S., Mitra K., Bhattacharya S., Chakrabarti R., Ray D. *et al.* (2017) Spectroscopic signature and geochemical constraints on jarosite formation at Kachchh: implications for Mars. Presented at: *Lunar and Planetary Science XLVIII*. The Woodlands, TX, USA, 20–24 March. Abstract 2270. Retrieved from https://www.researchgate.net/publication/313305405_SPECTROSCOPIC_SIGNATURE_AND_GEOCHEMICAL_CONSTRAINTS_ON_JAROSITE_FORMATION_AT_KACHCHH_IMPLICATIONS_FOR_MARS.

Moldoveanu G.A. & Papangelakis V.G. (2013) Recovery of rare earth elements adsorbed on clay minerals: II. Leaching with ammonium sulfate. *Hydrometallurgy*, **131–132**, 158–166.

Moldoveanu G.A. & Papangelakis V.G. (2016) An overview of rare-earth recovery by ion-exchange leaching from ion-adsorption clays of various origins. *Mineralogical Magazine*, **80**, 63–76.

Moldoveanu G. & Papangelakis V. (2021) Chelation-assisted ion-exchange leaching of rare earths from clay minerals. *Metals*, **11**, 1265.

Möller P. & Bau M. (1993) Rare-earth patterns with positive cerium anomaly in alkaline waters from Lake Van, Turkey. *Earth and Planetary Science Letters*, **117**, 671–676.

Moreira-Turcq P., Seyler P., Guyot J.L. & Etcheber H. (2003). Exportation of organic carbon from the Amazon River and its main tributaries. *Hydrological Processes*, **17**, 1329–1344.

Mozas T., Bruque S. & Rodríguez A. (1980) Effect of thermal treatment on lanthanide montomorillonites: dehydration. *Clay Minerals*, **15**, 421–428.

Nakada R., Waseda A., Okumura F. & Takahashi Y. (2016) Impact of the decarboxylation reaction on rare earth elements binding to organic matter: from humic substances to crude oil. *Chemical Geology*, **420**, 231–239.

Nakai S., Halliday A.N. & Rea D.K. (1993) Provenance of dust in the Pacific Ocean. *Earth and Planetary Science Letters*, **119**, 143–157.

Namayandeh A., Modabberi S. & López-Galindo A. (2020) Trace and rare earth element distribution and mobility during diagenetic alteration of volcanic ash to bentonite in eastern Iranian bentonite deposits. *Clays and Clay Minerals*, **68**, 50–66.

Nielsen D.L. & Hulen J.B. (1984) Internal geology and evolution of the Redondo Dome, Valles Caldera, New Mexico. *Journal of Geophysical Research: Solid Earth*, **89**, 8695–8711.

Ohta A., Kagi H., Tsuno H., Nomura M. & Kawabe I. (2008) Influence of multi-electron excitation on EXAFS spectroscopy of trivalent rare-earth ions and elucidation of change in hydration number through the series. *American Mineralogist*, **93**, 1384–1392.

Olivera-Pastor P., Rodríguez-Castellón E. & Rodríguez-García A. (1988) Uptakes of lanthanides by vermiculite. *Clays and Clay Minerals*, **36**, 68–72.

Parsapoor A., Khalili M. & Mackizadeh M.A. (2009) The behaviour of trace and rare earth elements (REE) during hydrothermal alteration in the Rangan area (central Iran). *Journal of Asian Earth Sciences*, **34**, 123–134.

Pérez-López R., Delgado J., Nieto J.M. & Márquez-García B. (2010) Rare earth element geochemistry of sulfide weathering in the São Domingos mine area (Iberian Pyrite Belt): a proxy for fluid–rock interaction and ancient mining pollution. *Chemical Geology*, **276**, 29–40.

Peterson K.A. & Dyall K.G. (2015) Gaussian basis sets for lanthanide and actinide elements. Pp. 195–216 in: M. Dolg (ed.), *Computational Methods in Lanthanide and Actinide Chemistry*. Wiley, Hoboken, NJ, USA.

Pi D.-H., Liu C.Q., Shields-Zhou G.A. & Jiang S.-Y. (2013) Trace and rare earth element geochemistry of black shale and kerogen in the early Cambrian Niutitang Formation in Guizhou province, South China: constraints for redox environments and origin of metal enrichments. *Precambrian Research*, **225**, 218–229.

Pipe A.B., Leybourne M.I., Johannesson K.H., Hannigan R.E. & Layton-Matthews D. (2025) Trace and rare earth element geochemistry of black shales from the Upper Ordovician Utica Shale magnafacies. *Chemical Geology*, **672**, 122507.

Piper D.Z. & Bau M. (2013) Normalized rare earth elements in water, sediments, and wine: identifying sources and environmental redox conditions. *American Journal of Analytical Chemistry*, **4**, 69–83.

Pourret O. & Tuduri J. (2017) Continental shelves as potential resource of rare earth elements. *Scientific Reports*, **7**, 5857.

Pourret O., Davranche M., Gruau G. & Dia A. (2007a) Competition between humic acid and carbonates for rare earth elements complexation. Journal of Colloid and Interface Science **305**, 25-31.

Pourret O., Davranche M., Gruau G. & Dia A. (2007b) Organic complexation of rare earth elements in natural waters: evaluating model calculations from ultrafiltration data. *Geochimica et Cosmochimica Acta*, **71**, 2718–2735.

Pourret O., Davranche M., Gruau G. & Dia A. (2008) New insights into cerium anomalies in organic-rich alkaline waters. *Chemical Geology*, **251**, 120–127.

Qiu S., Yan H., Hong B., Long Q., Xiao J., Li F. *et al.* (2022a) Desorption of *REE*s from halloysite and illite: a link to the exploitation of ion-adsorption *RE* ore based on clay species. *Minerals*, **12**, 1003.

Qiu Z., Tao C., Ma W., Dias Á.A., Hu S., Shao Y. *et al.* (2022b) Material source of sediments from West Clarion–Clipperton Zone (Pacific): evidence from rare earth element geochemistry and clay minerals compositions. *Journal of Marine Science and Engineering*, **10**, 1052.

Ramos S.J., Dinaly G.S., Oliveira C., Martins G.C., Moreira C.G., Siqueira J.O. & Guilherme L.R.G. (2016) Rare earth elements in the soil environment. *Current Pollution Reports*, **2**, 28–50.

Roaldset E. (1973) Rare earth elements in Quaternary clays of the Numedal area, southern Norway. *Lithos*, **6**, 349–372.

Romero F.M., Prol-Ledesma R.M., Canet C., Núñez Alvares L. & Pérez-Vázquez R. (2010) Acid drainage at the inactive Santa Lucia mine, western Cuba: natural attenuation of arsenic, barium and lead, and geochemical behavior of rare earth elements. *Applied Geochemistry*, **25**, 716–727.

Ruban A., Dudarev O., Rudmin M. & Semiletov I. (2024) Rare earth elements in sediments from the Laptev Sea shelf: insight into sources and distribution factors. *Quaternary*, **7**, 12.

Sasmaz A., Zuddas P., Cangemi M., Piazzese D., Ozek G., Venturi M. & Censi P. (2021) Zirconium and hafnium fractionation and distribution of rare earth elements in neutral–alkaline waters: case study of Lake Van hydrothermal system, Turkey. *Journal of Geochemical Exploration*, **226**, 106784.

Schijf J. & Byrne R.H. (2004) Determination of $_{SO4}\beta_1$ for yttrium and the rare earth elements at $I = 0.66$ m and $t = 25$°C – implications for *YREE* solution speciation in sulfate-rich waters. *Geochimica et Cosmochimica Acta*, **68**, 2825–2837.

Šegvić B., Badurina L., Braga A.E., Mandic O., Werts K., Doyle E. *et al.* (2024) Mobility patterns of rare earth elements in diagenetically altered vitric tuff shaped by illite-smectite. *Clays and Clay Minerals*, **72**, e14.

Seidel M., Dittmar T., Ward N.D., Krusche A.V., Richey J.E., Yager P.L. & Medeiros P.M. (2016) Seasonal and spatial variability of dissolved organic matter composition in the lower Amazon River. *Biogeochemistry*, **131**, 281–302.

Severmann S., Mills R.A., Palmer M.R. & Fallick A.E. (2004) The origin of clay minerals in active and relict hydrothermal deposits. *Geochimica et Cosmochimica Acta*, **68**, 73–88.

Shannon R.D. (1976) Revised effective ionic radii and systematic studies of interatomic distances in halides and chalcogenides. *Acta Crystallographica*, **A32**, 751–767.

Sharp J.H., Benner R., Bennett L., Carlson C.A., Fitzwater S.E., Peltzer E.T. & Tupas L.M. (1995) Analyses of dissolved organic carbon in seawater: the JGOFS EqPac methods comparison. *Marine Chemistry*, **48**, 91–108.

Shikazono N., Ogawa Y., Utada M., Ishiyama D., Mizuta T., Ishikawa N. & Kubota Y. (2008) Geochemical behavior of rare earth elements in hydrothermally altered rocks of the Kuroko mining area, Japan. *Journal of Geochemical Exploration*, **98**, 65–79.

Sholkovitz E.R. (1993) The geochemistry of rare earth elements in the Amazon River estuary. *Geochimica et Cosmochimica Acta*, **57**, 2181–2190.

Sholkovitz E.R. (1995) The aquatic chemistry of rare earth elements in rivers and estuaries. *Aquatic Geochemistry*, **1**, 1–34.

Slade P.G., Self P.G. & Quirk J.P. (1998) The interlayer structure of La-vermiculite. *Clays and Clay Minerals*, **46**, 629–635.

Spain A.V., Isbell R.F. & Probert M.E. (1983) Organic matter contents of Australian soils. Pp. 551–563 in: *Soils: An Australian Viewpoint*. CSIRO, Melbourne, Australia/Academic Press, London, UK.

Spirin R.V. (1965) *Rare Earth Distributions in the Marine Environment*. PhD thesis. MIT, Cambridge, MA, USA, 143 pp.

https://doi.org/10.1180/clm.2026.10030 Published online by Cambridge University Press

Stumpf T., Bauer A., Coppin F., Fanghänel T. & Kim J.I. (2002) Inner-sphere, outer-sphere and ternary surface complexes: a TRLFS study of the sorption process of Eu(III) onto smectite and kaolinite. *Radiochimica Acta*, **90**, 345–349.

Su N., Yang S., Guo Y., Yue W., Wang X., Yin P. & Huang X. (2017) Revisit of rare earth element fractionation during chemical weathering and river sediment transport. *Geochemistry, Geophysics, Geosystems*, **18**, 935–955,

Suta M., Fanica C. & Urland W. (2021) The angular overlap model of ligand field theory for f elements: an intuitive approach building bridges between theory and experiment. *Coordination Chemistry Reviews*, **441**, 213981.

Tachikawa K. & Barrat J.A. (2015) Rare earth elements and neodymium isotopes in world river sediments revisited. *Geochimica et Cosmochimica Acta*, **170**, 17–38.

Takahashi Y., Kimura T., Kato Y., Minai Y. & Tominaga T. (1998). Characterization of Eu(III) species sorbed on silica and montmorillonite by laser-induced fluorescence spectroscopy. *Radiochimica Acta*, **82**, 227–232.

Takahashi Y., Hirata T., Shimizu H., Ozaki T. & Fortin D. (2007) A rare earth element signature of bacteria in natural waters? *Chemical Geology*, **244**, 569–583.

Tang J. & Johannesson K.H. (2003) Speciation of rare earth elements in natural terrestrial waters: assessing the role of dissolved organic matter from the modeling approach. *Geochimica et Cosmochimica Acta*, **67**, 2321–2339.

Taylor S.R. & McLennan S.M. (1985) *The Continental Crust: Its Composition and Evolution: An Examination of the Geochemical Record Preserved in Sedimentary Rocks*. Blackwell Scientific Publications, Oxford, UK, 312 pp.

Tosca N.J. & Tutolo B.M. (2023) How to make an alkaline lake: fifty years of chemical divides. *Elements*, **19**, 15–21.

Tóth E., Weiszburg T.G., Jeffries T., Williams C.T., Bartha A., Bertalan E. & Cora I. (2010) Submicroscopic accessory minerals overprinting clay mineral *REE* patterns (celadonite–glauconite group examples). *Chemical Geology*, **269**, 312–328.

Trillo J.M., Alba M.D., Castro M.A., Muñoz A., Poyato J. & Tobías M.M. (1992) Local environment of lanthanum ions in montmorillonite upon heating. *Clay Minerals*, **27**, 423–434.

Tutolo B.M. & Tosca N.J. (2023) Dry, salty, and habitable: the science of alkaline lakes. *Elements*, **19**, 10–14.

USGS (2022) USGS mineral commodity summaries: rare earths. Retrieved from https://pubs.usgs.gov/periodicals/mcs2022/mcs2022-rare-earths.pdf.

Uysal I.T. & Golding S.D. (2003) Rare earth element fractionation in authigenic illite–smectite from Late Permian clastic rocks, Bowen Basin, Australia: implications for physico-chemical environments of fluids during illitization. *Chemical Geology*, **193**, 167–179.

van de Kamp P.C. (2019) Provenance, shallow to deep diagenesis, and chemical mass balance in supermature arenites and pelites, Ordovician Simpson Group, Oklahoma and Kansas, U.S.A. *Sedimentary Geology*, **386**, 79–102.

van der Does M., Korte L.F., Munday C.I., Brummer G.-J.A. & Stuut J.-B.W. (2016) Particle size traces modern Saharan dust transport and deposition across the Equatorial North Atlantic. *Atmospheric Chemistry and Physics*, **16**, 13697–13710.

Verplanck P.L., Nordstrom D.K., Taylor H.E. & Kimball B.A. (2004) Rare earth element partitioning between hydrous ferric oxides and acid mine water during iron oxidation. *Applied Geochemistry*, **19**, 1339–1354.

Viers J., Roddaz M., Filizola N., Guyot J.-L., Sondag F., Brunet P. *et al.* (2008) Seasonal and provenance controls on Nd-Sr isotopic compositions of Amazon rivers suspended sediments and implications for Nd and Sr fluxes exported to the Atlantic Ocean. *Earth and Planetary Science Letters*, **274**, 511–523.

Volkova N.I. (1998) Geochemistry of rare elements in waters and sediments of alkaline lakes in the Sasykkul Depression, East Pamirs. *Chemical Geology*, **147**, 265–277.

Welch S.A., Christy A.G., Isaacson L. & Kirste D. (2009) Mineralogical control of rare earth elements in acid sulfate soils. *Geochimica et Cosmochimica Acta*, **73**, 44–64.

Whitney G. (1990) Role of water in the smectite-to-illite reaction. *Clays and Clay Minerals*, **38**, 343–350.

Williams-Jones A.E., Migdisov A.A. & Samson I.M. (2012) Hydrothermal mobilisation of the rare earth elements – a tale of 'ceria' and 'yttria'. *Elements*, **8**, 355–360.

Wu Z., Chen Y., Wang Y., Xu Y., Lin Z., Liang X. & Cheng H. (2023) Review of rare earth element (*REE*) adsorption on and desorption from clay minerals: application to formation and mining of ion-adsorption *REE* deposits. *Ore Geology Reviews*, **157**, 105446.

Xing B. & Dudas M.J. (1993) Trace and rare earth element content of white clay soils of the Three River Plain, Heilongjiang Province, P.R. China. *Geoderma*, **58**, 181–199.

Xu Z., Lim D., Choi J., Yang S. & Jung H. (2009) Rare earth elements in bottom sediments of major rivers around the Yellow Sea: implications for sediment provenance. *Geo-Marine Letters*, **29**, 291–300.

Yamaguchi A., Honda T., Tanaka M., Tanaka K. & Takahashi Y. (2018) Discovery of ion-adsorption type deposits of rare earth elements (*REE*) in Southwest Japan with speciation of *REE* by extended X-ray absorption fine structure spectroscopy. *Geochemical Journal*, **52**, 415–425.

Zhang X., Jing Y., Zhao W., Jiang Y., Guan D.-X., Du H. *et al.* (2024) Rare earth elements in clay-sized fractions: implications for weathering fingerprint from parent materials to soils. *Geoderma*, **445**, 116879.

Zhao G., Deng Q., Fang X., Wang H., Cheng B. & Liao Z. (2023) Towards deciphering the source of rare earth elements in kerogen: seawater or diagenetic porewater origin? *Chemical Geology*, **641**, 121783.

https://doi.org/10.1180/clm.2026.10030 Published online by Cambridge University Press